Iron sources and dissolved-particulate interactions in the seawater of the Western Equatorial Pacific, iron isotope perspectives

M Labatut, F. Lacan, C Pradoux, J Chmeleff, A Radic, James W. Murray, F Poitrasson, A. M. Johansen, F Thil

AGU PUBLICATIONS

Global Biogeochemical Cycles

RESEARCH ARTICLE
10.1002/2014GB004928

Key Points:
- Isotopic composition of dissolved and particulate Fe in seawater
- Isotopic composition of Fe in marine aerosol, Sepik, and margin sediments
- Nonreductive release would be an important source of dissolved Fe

Correspondence to:
M. Labatut,
marie.labatut@legos.obs-mip.fr

Citation:
Labatut, M., F. Lacan, C. Pradoux, J. Chmeleff, A. Radic, J. W. Murray, F. Poitrasson, A. M. Johansen, and F. Thil (2014), Iron sources and dissolved-particulate interactions in the seawater of the Western Equatorial Pacific, iron isotope perspectives, *Global Biogeochem. Cycles*, *28*, 1044–1065, doi:10.1002/2014GB004928.

Received 1 JUL 2014
Accepted 31 AUG 2014
Accepted article online 3 SEP 2014
Published online 10 OCT 2014

Iron sources and dissolved-particulate interactions in the seawater of the Western Equatorial Pacific, iron isotope perspectives

M. Labatut[1], F. Lacan[1], C. Pradoux[1], J. Chmeleff[2], A. Radic[1], J. W. Murray[3], F. Poitrasson[2], A. M. Johansen[4], and F. Thil[5]

[1]Laboratoire des Etudes en Géophysique et Océanographie Spatiale, Observatoire Midi-Pyrénées, CNES/CNRS/IRD/University of Toulouse, France, [2]Laboratoire Géosciences Environnement Toulouse, Observatoire Midi-Pyrénées, CNRS/IRD/University of Toulouse, France, [3]School of Oceanography, University of Washington, Seattle, Washington, USA, [4]Central Washington University, Elensburg, Washington, USA, [5]Laboratoire des Sciences du Climat et de l'Environnement, CNRS/CEA/UVSQ, Gif-sur-Yvette, France

Abstract This work presents iron isotope data in the western equatorial Pacific. Marine aerosols and top core margin sediments display a slightly heavy Fe isotopic composition (δ^{56}Fe) of 0.33 ± 0.11‰ (2SD) and 0.14 ± 0.07‰, respectively. Samples reflecting the influence of Papua New Guinea runoff (Sepik River and Rabaul volcano water) are characterized by crustal values. In seawater, Fe is mainly supplied in the particulate form and is found with a δ^{56}Fe between −0.49 and 0.34 ± 0.07‰. The particulate Fe seems to be brought mainly by runoff and transported across continental shelves and slopes. Aerosols are suspected to enrich the surface Vitiaz Strait waters, while hydrothermal activity likely enriched New Ireland waters. Dissolved Fe isotopic ratios are found between −0.03 and 0.53 ± 0.07‰. They are almost systematically heavier than the corresponding particulate Fe, and the difference between the signature of both phases is similar for most samples with $\Delta^{56}Fe_{DFe-PFe} = +0.27 \pm 0.25$‰ (2SD). This is interpreted as an equilibrium isotopic fractionation revealing exchange fluxes between both phases. The dissolved phase being heavier than the particles suggests that the exchanges result in a net nonreductive release of dissolved Fe. This process seems to be locally significantly more intense than Fe reductive dissolution documented along reducing margins. It may therefore constitute a very significant iron source to the ocean, thereby influencing the actual estimation of the iron residence time and sinks. The underlying processes could also apply to other elements.

1. Introduction

Iron availability is a limiting factor for phytoplankton growth in the High Nutrient Low Chlorophyll (HNLC) areas of the world ocean, notably in the eastern equatorial Pacific Ocean [*Martin*, 1990; *Boyd et al*., 2007]. Variations of Fe inputs to the ocean are thought to impact the global carbon cycle and climate. Despite this importance, many aspects of the Fe oceanic cycle remain unknown. In particular, significant uncertainties remain about the sources of Fe to the open ocean and about exchanges between its particulate and dissolved pools.

Iron distribution in the ocean results from its sources, sinks, and internal cycling. Sinking particles constitute the only sink that removes Fe from water column, whereas there are numerous Fe sources. Several Fe sources to the open ocean have been proposed, and they are currently being debated. Whereas dust dissolution has long been considered as the predominant source [*Duce and Tindale*, 1991; *Jickells et al*., 2005], sediment dissolution and resuspension along continental margins have been also proposed to contribute significantly to the Fe content of the open ocean [*Coale et al*., 1996; *Elrod et al*., 2004; *Blain et al*., 2008; *Moore and Braucher*, 2008; *Tagliabue et al*., 2009; *Ardelan et al*., 2010; *Jeandel et al*., 2011; *Radic et al*., 2011]. Riverine inputs [*De Baar and De Jong*, 2001] and hydrothermal inputs [*Boyle and Jenkins*, 2008; *Boyd and Ellwood*, 2010; *Tagliabue et al*., 2010] are also significant contributors to the Fe content of the global ocean. Although probably representing smaller contributions, Fe could be supplied from groundwater, volcanic eruptions, glacial/iceberg melt, extraterrestrial dust, or anthropogenic emissions [*Windom et al*., 2006; *Sedwick et al*., 2007; *Smith et al*., 2007; *Luo et al*., 2008].

The iron isotopic compositions may differ depending on the source (Figure 1) [*Beard and Johnson*, 2004; *Severmann et al*., 2006]. Consequently, Fe isotopes constitute a pertinent tool for study of Fe sources to the

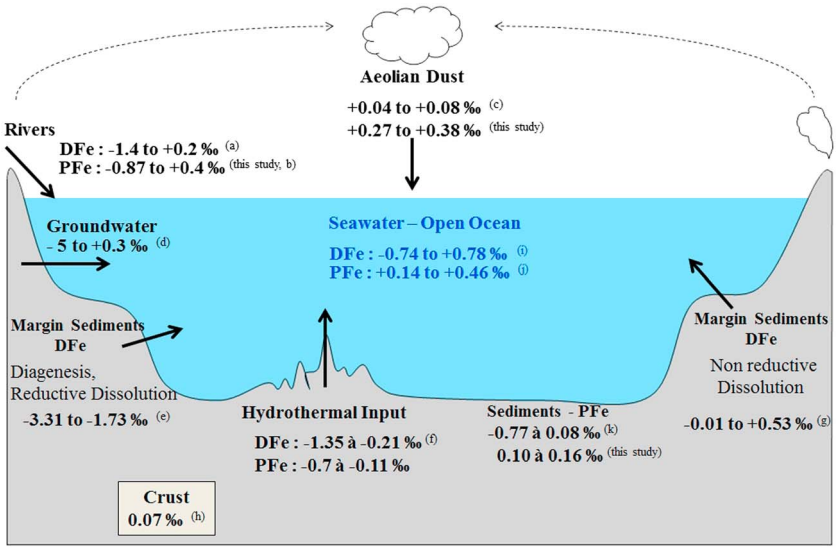

Figure 1. Schematic diagrams illustrating the isotopic composition of Fe inputs to the ocean (‰) and that of seawater. PFe and DFe are, respectively, for particulate Fe and Dissolved Fe. Letters in parenthesis indicate the associated references: (a) *de Jong et al.* [2007], *Chen et al.* [2014], *Escoube et al.* [2009], and *Poitrasson et al.* [2014]; (b) *Ingri et al.* [2006], *de Jong et al.* [2007], *Escoube et al.* [2009], *dos Santos Pinheiro et al.* [2013], and *Chen et al.* [2014]; (c) *Beard et al.* [2003a], *Beard and Johnson* [2004], *Fantle and DePaolo* [2004], and *Waeles et al.* [2007]; (d) *Rouxel et al.* [2008b]; (e) *Severmann et al.* [2006, 2010] and *Homoky et al.* [2009]; (f) *Sharma et al.* [2001], *Beard et al.* [2003a], *Rouxel et al.* [2008a], and *Bennett et al.* [2009]; (g) *Homoky et al.* [2009, 2013] and *Radic et al.* [2011]; (h) *Poitrasson* [2006]; (i) *Lacan et al.* [2008], *Radic et al.* [2011], *John and Adkins* [2012], *Conway et al.* [2013], and Abadie et al. (submitted manuscript, 2014); (j) Abadie et al. (submitted manuscript, 2014) and *Radic et al.* [2011]; (k) *Fantle and DePaolo* [2004], *Severmann et al.* [2006], *Staubwasser et al.* [2006], and *Homoky et al.* [2013].

ocean [*Lacan et al.*, 2008; *John and Adkins*, 2010]. The Fe isotopic composition is expressed by δ^{56}Fe in ‰ and defined relative to the international reference material IRMM-14 as

$$\delta^{56}\mathrm{Fe} = \left[\frac{\left(^{56}\mathrm{Fe}/^{54}\mathrm{Fe}\right)_{\mathrm{sample}}}{\left(^{56}\mathrm{Fe}/^{54}\mathrm{Fe}\right)_{\mathrm{IRMM-14}}} - 1\right]\cdot 10^{3} \quad (1)$$

The continental crust has a signature of $\delta^{56}\mathrm{Fe} = 0.07 \pm 0.02$‰ [*Poitrasson*, 2006]. Atmospheric dust sampled close to arid regions has been characterized by an Fe isotopic composition undistinguishable from that of the continental crust: $\delta^{56}\mathrm{Fe} = 0.04‰ \pm 0.09‰$ to $0.08‰ \pm 0.08‰$ [*Beard et al.*, 2003a; *Beard and Johnson*, 2004; *Fantle and DePaolo*, 2004; *Waeles et al.*, 2007]. So far, no isotopic measurement of marine aerosol sampled in the open ocean has been performed. In areas of high primary production, where organic matter degradation is intense, pore waters in sediments deposited on continental shelves and upper slopes display a light dissolved Fe (DFe) isotopic composition, $\delta^{56}\mathrm{DFe} = -3.31$ to -1.73 ± 0.08‰ [*Severmann et al.*, 2006, 2010; *Homoky et al.*, 2009]. This negative signal reflects the reduction of Fe^{III} to Fe^{II} in the sediments during diagenesis [*Severmann et al.*, 2006]. More recently, positive values of DFe found close to continental margins, with $\delta^{56}\mathrm{DFe} = 0.06$ to 0.53 ± 0.08‰, were suggested to reflect another process of Fe release from the sediments, the nonreductive release [*Radic et al.*, 2011; *Homoky et al.*, 2013]. This nonreductive release is supported by positive Fe isotopic signature of pore waters from sediments in areas with low organic matter degradation [*Homoky et al.*, 2009, 2013]. Slightly light δ^{56}Fe values between -0.5 and -0.21‰, for dissolved Fe, and between -0.7 and -0.11‰ in the particulate fraction have been measured in hydrothermal fluids [*Sharma et al.*, 2001; *Beard et al.*, 2003a; *Rouxel et al.*, 2008a; *Bennett et al.*, 2009]. A light signature has also been measured for DFe in a buoyant hydrothermal plume, with $\delta^{56}\mathrm{Fe} = -1.3$‰ [*Conway and John*, 2014]. These results suggest that hydrothermal vents are a source of isotopically light DFe and PFe to the oceans. Some studies have characterized dissolved δ^{56}Fe of other sources that may contribute locally to a significant iron flux. For instance, for river inputs, a δ^{56}DFe ranged from -1.4 to 0.2‰ was measured within river waters in the Amazon River, the Seine, and the Scheldt estuary [*De Jong et al.*, 2007; *Chen et al.*, 2014; *Poitrasson et al.*, 2014]. The suspended matter signature ranged from -0.87 to 0.4‰ [*Ingri et al.*, 2006; *de Jong et al.*, 2007; *Escoube et al.*, 2009; *dos Santos Pinheiro et al.*, 2013; *Chen et al.*, 2014]. During the flocculation in

estuarine environments, no significant change of the δ^{56}DFe was observed in the North River estuary (USA), with an average value of +0.43‰ [*Escoube et al*., 2009]. Nevertheless, a decreasing, down to −1.2‰, was observed in the Scheldt estuary [*De Jong et al*., 2007]; this decreasing could be due to flocculation or groundwater discharges. Dissolved Fe inputs from groundwater may be very light (from −5‰ up to 0.3‰) [*Rouxel et al*., 2008b].

Most of the research on biogeochemical cycle of Fe has focused on dissolved Fe or total Fe [*Martin et al*., 1989; *Johnson et al*., 1997; *de Baar and de Jong*, 2001; *Wu and Boyle*, 2002] despite the fact that total Fe is dominated by the particulate fraction in the surface mixed layer [*De Baar and De Jong*, 2001] and in coastal area [*Radic et al*., 2011; Abadie et al., Iron isotopes evidence different dissolved iron sources in the intermediate and deep Ocean, submitted to *Nature Geosciences*, 2014]. However, dissolved Fe (DFe) and particulate Fe (PFe) interact with each other through numerous processes that could fractionate iron, notably processes of biological uptake, remineralization, adsorption/desorption, and dissolution/precipitation [*Ussher et al*., 2004]. It is thus necessary to study both dissolved and particulate Fe to improve our understanding of its biogeochemical cycle. Few studies have provided the isotopic composition of dissolved Fe in seawater and even fewer of particulate Fe. Coastal seawater samples display δ^{56}DFe from -1.82 ± 0.06‰ to 0.53 ± 0.14‰ [*De Jong et al*., 2007; *Radic et al*., 2011; *John et al*., 2012; *Staubwasser et al*., 2013] and δ^{56}PFe from −0.61 to 0.7‰ [*De Jong et al*., 2007; *Radic et al*., 2011; *Staubwasser et al*., 2013]. In the open ocean where DFe and PFe concentrations are very low compared to the coastal environment, δ^{56}DFe ranges from 0.14 ± 0.13‰ to 0.74 ± 0.07‰ in the North Atlantic [*John and Adkins*, 2012; *Conway et al*., 2013], from −0.71 to 0.47 ± 0.08‰ in the South Eastern Atlantic [*Lacan et al*., 2008; Abadie et al., submitted manuscript, 2014] and from 0.01 to 0.58 ± 0.08‰ in the equatorial Pacific [*Radic et al*., 2011]. Particulate iron isotopic compositions range from δ^{56}PFe = 0.14 to 0.46 ± 0.08‰ in the equatorial Pacific [*Radic et al*., 2011] and from −0.04 to 0.32‰ in the South Eastern Atlantic (Abadie et al., submitted manuscript, 2014). Published data are very scarce (19 data for δ^{56}DFe and 6 for δ^{56}PFe) and scattered (four profiles of δ^{56}DFe and one of δ^{56}PFe for the open ocean) in the global ocean. In this study, new profiles of δ^{56}DFe and δ^{56}PFe are presented in order to characterize how Fe isotopes are exchanged between the particulate and dissolved reservoirs in coastal seawater.

The equatorial Pacific circulation is fed by a redistribution of waters from the open ocean subtropical gyres toward the Equatorial Undercurrent (EUC), mainly via the low-latitude western boundary currents [*Fine et al*., 1994; *Grenier et al*., 2011] (Figure 2). The EUC carries thermocline waters along the equator [*Lukas and Firing*, 1984] from the Western to the Eastern equatorial Pacific HNLC area [*Behrenfeld et al*., 1996]. Several studies have concluded that the EUC is enriched in micronutrients in the Western coastal part of the equatorial Pacific, in particular along Papua New Guinea coast [*Johnson and McPhaden*, 1999; *Lacan and Jeandel*, 2001; *Mackey et al*., 2002; *Slemons et al*., 2009, 2010; *Radic et al*., 2011]. Upwelling of waters transported by EUC controls micronutrient supply to the surface ocean, modulating primary production in the HNLC area of the eastern equatorial Pacific [*Coale et al*., 1996; *Ryan et al*., 2006; *Slemons et al*., 2009]. The 2006 EUCFe cruise (R/V *Kilo Moana*) conducted trace element sampling to link the western source region to the central equatorial Pacific (Figure 3). *Slemons et al*. [2010, 2012] showed that there was a maximum of total Fe, mainly composed of PFe, associated with the EUC which increased toward the West. This result is consistent with the Western source hypothesis. From one profile located downstream the Sepik River off Papua New Guinea, *Radic et al*. [2011] proposed that this dissolved Fe is mainly released from the sediments via nonreductive processes, but is it true throughout the Bismarck Sea? What are the other potential sources? What are the associated fluxes? How do the exchanges between the dissolved and the particulate pool occur? What are the isotopic fractionations during these exchanges? This study aims to provide answers to such questions using the isotopic approach.

2. Hydrological Context

The Western equatorial Pacific is a transit area for Western boundary currents before their input into the equatorial currents [*Fine et al*., 1994]. This basin is bordered by Papua New Guinea and Australia, and numerous scattered islands (Figure 3). This geographic distribution coupled with a rough topography leads to a complex circulation summarized on Figure 2. When the water masses such as thermocline and central waters (Table 1) transported by the South and North Westward currents reach the coast, these water masses then enter in the low-latitude western boundary currents flowing toward the Equator, such as the New

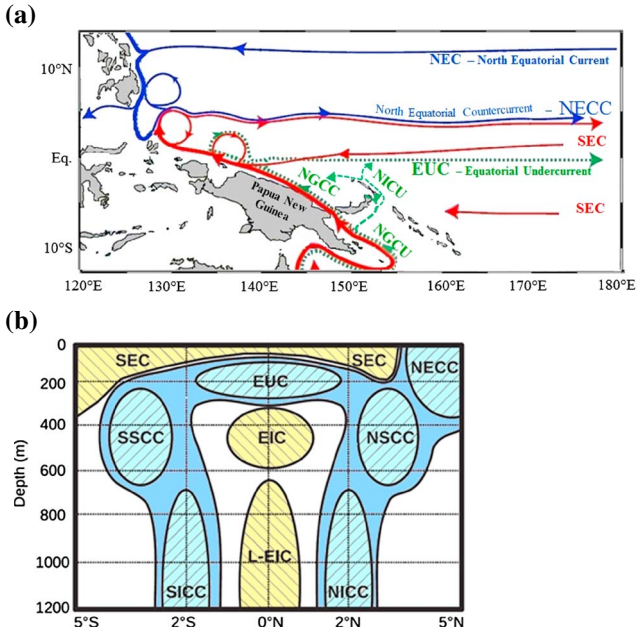

Figure 2. Equatorial circulation (currents) of the Western Pacific Ocean (a) on a map and (b) on a meridional section at 180°E. In Figure 2a, blue arrows represent the water masses of the northern hemisphere, red arrows that of the southern hemisphere, and green arrows represent the undercurrents. In Figure 2b, eastward flows are in blue, and westward flows are in yellow. Shaded areas represent strong currents. SEC = South Equatorial Current; NGCC = New Guinea Coastal Countercurrent; NGCU = New Guinea Coastal Undercurrent; NICU = New Ireland Coastal Undercurrent; NECC = North Equatorial CounterCurrent; SSCC and NSCC = North and South Subsurface Countercurrents; EUC = Equatorial UnderCurrent; EIC = Equatorial Intermediate Current; L-EIC = Lower-EIC; SICC and NICC = South and North Intermediate CounterCurrents [from *Tomczak and Godfrey*, 2003; *Delcroix et al.*, 1992; *Fine et al.*, 1994; *Johnson et al.*, 2002; *Kashino et al.*, 1996, 2007].

Guinea Coastal Undercurrent and Countercurrent and the New Ireland Coastal Undercurrent (Figure 2a). When these water masses reach the equator, they enter in the Equatorial Undercurrent (EUC) (Figure 2). Deeper, intermediate waters (Table 1 and Figure 2b) flow more slowly in eastward currents such as the Equatorial Intermediate Current. At the surface, waters are driven by the Easterly winds and renewed by the equatorial upwelling [*Gordon et al.*, 1997].

3. Sampling and Methods

3.1. Seawater Sampling

Seawater samples were collected during the EUCFe cruise (August–October 2006, R/V *Kilo Moana*) (Figure 3), from 25 to 1000 m depth. The conductivity, temperature, depth (CTD), chlorophyll a, oxygen, and nutrient data are available online (http://www.ocean.washington.edu/cruises/KiloMoana2006/).

Seawater was sampled with 12 L acid-cleaned Go-Flo bottles mounted on a trace-metal rosette equipped with a CTD (lent by Canadian GEOTRACES, University of Victoria, Canada, and assembled at the University of Washington, USA [*Slemons et al.*, 2010]). The bottles were brought into a homemade plastic room

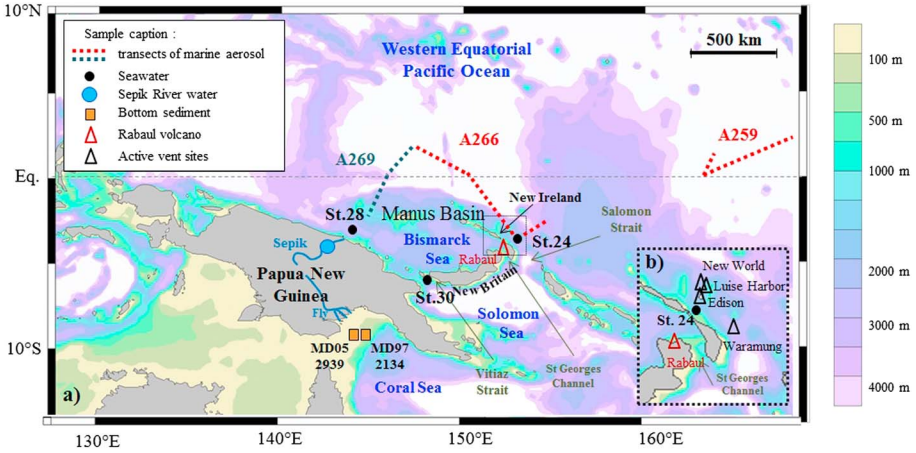

Figure 3. (a) Maps of the Western Equatorial Pacific. (b) Zoom on the New Ireland. Depths higher than 4000 m are white. The sampling transects of marine aerosols are represented with colored dotted lines. Black dots are the sampling location of seawater; the blue dot is the sampling location of Sepik River water; orange squares are the sediment sampling locations; red triangle represents the sampling location of surface seawater at the base of one of the several still active volcanoes, the Rabaul Volcanoes; black triangles represent active hydrothermal vents (http://www.interridge.org, no sample).

Table 1. Acronyms of Water Masses Present in the Study Area, With Their Characteristics: Origin, Potential Temperature (°C), density (kg/m3), Oxygen Concentration (μmol/kg), and Salinity[a]

Water Masses									
	Acronym	Meaning	Origin	Potential Temperature θ (°C)	Density (kg/m^3)	Oxygen (μmol/kg)	Salinity	Currents	References
Thermocline Waters	NPEW	North Pacific Equatorial Water	Bondary between subtropical gyres	18–20	24.3–25.3		34.9	NECC, EUC	*Tomczak and Godfrey*, 2003
	NPTW	North Pacific Tropical Water	North subtropical area		24.3–25.3		35.3–35.4	NEC, EUC	*Tsuchiya et al.*, 1989
	SPEW	South Pacific Equatorial Water	Subduction of surface waters in the tropics	18–20	24.3–25.3	140	35.6–35.8	NICU, EUC	*Tomczak and Hao*, 1989; *Tsuchiya et al.*, 1989; *Qu and Lindstrom*, 2002; *Cravatte et al.*, 2011
	SPTW	South Pacific Tropical Water	South subtropical area	18–25	24.3–25.3	<160	36.4–36.7	SEC, NGCU /NGCC, NICU/NGCU, EUC	*Tsuchiya et al.*, 1989
Central Waters	WNPCW	Western North Pacific Central Water	Northern subtropical front	10–17	25.2–26.4	<160	33.5–34.5	NECC, EUC	*Pickard and Emery*, 1990; *Tomczak and Godfrey*, 2003
	WSPCW	Western South Pacific Central Water	Subtropical convergence zone between Tasmania and New Zealand	10–17	26.1–26.7	160	35–35.5	SEC, NGCU /NGCC, NICU/NGCU, EUC	*Tsuchiya*, 1981; *Qu and Lindstrom*, 2002; *Tomczak and Godfrey*, 2003; *Sokolov and Rintoul*, 2007; *Qu et al.*, 2009
Intermediate Waters	AAIW	AntArctic Intermediate Water	Subantarctic front	3–6	27.1–27.3	160–300	34.3–34.5	NGCU, EIC, NSCC, SSCC	*Tsuchiya and Talley*, 1998
	NPIW	North Pacific Intermediate Water	Front between the Kuroshio and the Oyashio current	3–6	26.5–27.3	0–150	33.5–34.1	NGCU, EIC, NSCC, and SSCC	*Talley*, 1993; *Fine et al.*, 1994; *You*, 2003

[a]The currents where they flow are also specified (see Figure 2 for acronym meaning).

pressurized with filtered air. Within 4 h after collection, the samples were filtered through acid-cleaned Nuclepore® membranes (0.4 μm pore size, 90 mm diameter), fitted in acid-cleaned Savillex PTFE filter holders, and connected with PTFE tubing to the Go-Flo bottles pressurized with filtered air (0.2 μm). Ten liters of filtered seawater were transferred to an acid-cleaned polyethylene container, and protected from light and dusts with a black bag. The Nuclepore® membranes were preserved in an acid-cleaned petri dish.

Note that the Fe concentrations and isotopic compositions from station 28 have been previously measured and published by *Radic et al.* [2011]. The present work presents new data for DFe and PFe from stations 24 and 30, together with two additional PFe data points from station 28 (Table 2).

3.2. Analytical Chemical Treatment for Filtered Water and Particles

All chemical separations were conducted in a trace metal clean lab and under an ISO4 (class 10) laminar flow hood. Trace metal clean reagents were used (Suprapur® or twice distilled at LEGOS). All labware were acid cleaned. Blanks of reagents, labware, and atmosphere were regularly monitored.

The procedure used for determination of the isotopic composition of dissolved Fe in seawater was fully described in *Lacan et al.* [2008, 2010], and it is summarized below. Filtered seawater was acidified to pH 1.80 a few months before beginning the chemical extractions. A double-spike solution of ^{57}Fe–^{58}Fe was added to each sample in order to correct for isotopic fractionations potentially induced by the entire procedure. Just before the preconcentration, hydrogen peroxide was added to oxidize Fe^{II} to Fe^{III} [*Strelow*, 1980;

AGU Global Biogeochemical Cycles

10.1002/2014GB004928

Table 2. Locations, Depths, Hydrological Properties (see the EUCFe Website for More Information http://www.ocean.washington.edu/cruises/KiloMoana2006/), Isotopic Composition (‰), and Concentration (nM or nmol.kg^{-1}) of Dissolved and Particulate Fe (DFe and PFe)[a]

GoFlo bottle	Depth (m)	θ (°C)	Salinity	[O2] (μmol/kg)	θσ (kg/m3)	Water mass	Dissolved Fraction				Particulate Fraction			
							Replicates	[DFe] (nM)	δ^{56}DFe (‰)	2SD (‰)	Replicates	[PFe] (nM)	δ^{56}PFe (‰)	2SD (‰)
STATION 24 (3.2°S, 152.3°E, cast TM47, 23 September 2006, bottom = 1669 m)														
2	920	4.6	34.52	141	27.34	AAIW	α_5	0.99	0.34	0.07	α_4	4.91	−0.05	0.09
											β	4.90	0.04	0.07
											Mean	*4.91*	*0.00*	
5	370	10.5	34.78	(*) 143 ± 9	26.70	CW	a, α_5	0.70	0.24	0.07	α_4	4.88	−0.05	0.12
							b, α_5	0.64	0.30	0.07	β	4.87	−0.01	0.07
							Mean	*0.67*	*0.27*		*Mean*	*4.87*	*−0.03*	
7	180	19.9	35.57	133	25.22	SPTW	α_5	0.86	−0.03	0.07	α_4	7.82	−0.48	0.10
											β	7.80	−0.49	0.07
											Mean	*7.81*	*−0.48*	
9	65	27.4	34.74	196	22.38	Chloro. Max.	α_5	0.30	0.20	0.07	α_4	1.66	0.03	0.16
											β	1.65	−0.01	0.07
											Mean	*1.66*	*0.01*	
11	40	28.7	34.56	199	21.83	Surface Waters	α_5	0.48	−0.03	0.07	α_4	1.15	0.18	0.13
											β	1.14	0.08	0.07
											Mean	*1.15*	*0.13*	
STATION 28 (3.4°S, 143.9°E, cast TM56, 28 September 2006, bottom = 2256 m)														
2	799	5.5	34.50	151	27.22	AAIW	1, α_1 †	1.46	0.06	0.07	α_2 †	9.62	−0.02	0.09
							2, α_1 †	1.46	0.08	0.08	β	8.96	−0.03	0.07
							3, α_1 †	1.46	0.02	0.07				
							4, α_1 †	1.46	0.07	0.08				
							Mean	*1.46*	*0.06*		*Mean*	*8.96*	*−0.03*	
5	321	13.8	35.09	154	26.31	CW	α_1 †	0.77	0.29	0.07	α_2 †	7.34	0.04	0.07
7	191	19.1	35.45	145	25.33	SPTW	1, α_1 †	0.67	0.45	0.08	α_2 †	6.91	0.29	0.07
							2, α_1 †	0.67	0.42	0.08				
							Mean	*0.67*	*0.43*					
8	94	26.5	34.85	180.9	22.77	Chloro. Max.	a, α_1 †	0.45	0.36	0.07	α_2 †	4.63	—	—
							b, α_1 †	0.45	0.44	0.08	β	4.65	0.01	0.07
							Mean	*0.45*	*0.40*		*Mean*	*4.64*	*0.01*	
10	40	27.5	34.70	196.6	22.32	Surface Waters	α_1 †	0.89	0.53	0.07	a, α_5	29.45	0.02	0.07
											b, 1, α_5	29.45	0.06	0.07
											b, 2, α_5	29.45	0.04	0.07
											Mean	*29.45*	*0.04*	
STATION 30 (5.6°S, 147.4°E, cast TM61, 30 September 2006, bottom = 1040 m)														
B2	916	4.6	34.51	(*) 143 ± 16	27.33	AAIW	α_3	1.19	—	—	1, α_4	7.62	—	—
							α_4	1.20	—	—	2, α_4	7.62	−0.03	0.07
							β	1.23	—	—	1, β	7.62	−0.03	0.07
											2, β	7.62	−0.05	0.07
							Mean	*1.21*	—		*Mean*	*7.62*	*−0.03*	
B3	730	5.9	34.48	(*) 166 ± 16	27.15	AAIW	α_3	0.94	—	—	α_4	3.22	—	—
							α_4	0.92	0.43	0.12	β	3.23	0.01	0.07
							β	0.95	0.44	0.07				
							Mean	*0.94*	*0.44*		*Mean*	*3.23*	*0.01*	
B6	350	11.8	34.92	(*) 162 ± 16	26.57	CW	α_5	0.48	0.31	0.07	1, α_4	3.90	0.20	0.07
											2, β	3.90	0.20	0.07
											Mean	*3.90*	*0.20*	

Table 2. (continued)

GoFlo bottle	Depth (m)	θ (°C)	Salinity	[O2] (µmol/kg)	θσ (kg/m3)	Water mass	Dissolved Fraction				Particulate Fraction			
							Replicates	[DFe] (nM)	δ^{56}DFe (‰)	2SD (‰)	Replicates	[PFe] (nM)	δ^{56}PFe (‰)	2SD (‰)
B7	200	18.7	35.53	(*) 144 ± 16	25.49	SPTW	α_3	0.65	—	—	1, α_4	3.72	—	—
							α_4	0.65	0.44	0.10	2, α_4	3.72	—	—
							β	0.66	0.39	0.07	1, β	3.73	0.20	0.07
											2, β	3.73	0.15	0.07
							Mean	*0.65*	*0.41*		*Mean*	*3.72*	*0.17*	
B10	25	27.3	34.76	(*) 200 ± 4	22.44	Surface Waters	α_3	0.13	—	—	a, 1, α_4	0.44	—	—
											a, 2, α_4	0.44	—	—
											a, 3, β	0.44	0.34	0.08
											a, 4, β	0.44	0.27	0.07
											b, α_5	0.46	0.28	0.07
											Mean	*0.44*	*0.30*	

[a]The measurement uncertainty is ±0.07‰ (2SD) or the 2SE when 2SE is larger than 0.07‰. Each kind of replicates is notified with the following symbols: a,b,c symbolize the chemical replicates (samples divided into two or three parts, such that each contain ~150 ng of Fe, before preconcentration for dissolved samples and before purification for particulate samples, and each part was analyzed independently) ; 1, 2, 3 symbolize the measurement replicates (the same sample measured several times during the same session); α and β symbolize the machine replicates (α when sample was measured on the MC-ICPMS of the *Observatoire Midi Pyrénées* (OMP) and β when sample was measured on the MC-ICPMS of the *Laboratoire des Sciences du Climat et de l'Environnement* (LSCE); α_1, α_2, α_3, α_4, α_5 are for different measurement sessions on the MC-ICPMS of OMP). The dissolved O_2 concentration was generally directly measured in seawater samples onboard, sometimes not. In the latter case specified by the (*) symbol, the concentration given by the oxygen sensor mounted on the rosette is used after calibration against in situ data. Symbol (†) pertains to previously published data by *Radic et al.* [2011]. CW = Central Water; SPTW = South Pacific Tropical Water; AAIW = Antarctic Intermediate Water; Chloro. Max = Chlorophyll Maximum layer.

Lohan et al., 2005]. The filtered seawater was preconcentrated with a NTA Superflow resin (Qiagen®). The average recovery of this step was 92 ± 25% (2SD, $n = 55$), and the blank was 0.17 ± 0.44 ng (2SD, $n = 10$).

To determine the concentration and the isotopic composition of particulate Fe, the Nuclepore® membranes were first leached using the method described in *Radic et al.* [2011]. The filters were covered with 18 ml of an acid mixture (HCl 5 M, HNO_3 2.1 M, HF 0.6 M) and heated to 130°C for 3 h in closed PTFE vials (Lacan et al., Chemical composition of suspended particles in the Atlantic sector of the southern ocean, in preparation, 2015). The filters were taken out of the digestion solution, rinsed with Milli-Q Element® water, and a ^{57}Fe–^{58}Fe double-spike was added to each sample. Some filters were leached again to check that the procedure was efficient. No PFe could be detected in the second leach. Blank for this PFe treatment was of 5.9 ± 4.1 ng (2SD, $n = 7$).

Then, the particulate and dissolved iron samples underwent the same procedure. Around 2% of each sample was aliquoted to carry out a first measurement of Fe and other elements concentrations (Na, Mg, K, Al, Ti, etc.) by High Resolution Inductively Coupled Plasma Mass Spectrometer (HR-ICPMS) Element (Thermo Scientific®). Residues of the particulate and dissolved samples were purified twice with an AG1-X4 anionic resin (200–400 mesh). Average recovery of one purification step was 96 ± 18% (2SD, $n = 20$). The blank was 0.61 ± 0.81 ng (2SD, $n = 17$).

Total yield for the entire procedure was 93 ± 25% for PFe and 86 ± 33% for DFe. Putative isotopic fractionation sometimes associated with low yields was here corrected by the addition of a double spike in the samples prior to the chemical procedure. The mean concentrations of PFe and DFe in samples were, respectively, 1.5 nM and 0.5 nM. The lowest values of PFe and DFe concentration reach 0.15 nM and 0.05 nM. The blank fraction was on average 0.8% for PFe and 0.5% for DFe, and at most 9% for PFe and 5% for DFe.

3.3. Analytical Chemical Treatment for Other Kind of Samples

3.3.1. Dusts

Atmospheric particles were collected on board on the R/V *Kilo Moana* by *Shank and Johansen* [2008] continuously during the EUCFe cruise (Figure 3). The three samples analyzed here were sampled with a small volume collector equipped with 47 mm diameter Millipore® polycarbonate filter holders and acid-cleaned PTFE filters having a porosity of 1 μm. The pumped air flow was measured with a flow meter. To protect aerosols from rain, the filter support was pointing downward and covered with a plastic cover. To avoid contamination from ship smoke, the collector was located on the top deck above the bridge. It was also equipped with a control system which allowed pumping to stop when the wind came from a direction greater than 60° from the bow. In a clean lab, dust samples were analyzed with exactly the same protocol as particles. Blank of this PFe treatment was 5.9 ± 4.1 ng (2SD, $n = 7$).

3.3.2. Sepik River

One liter of Sepik river water was sampled at Angoram (4°03′S 144°04′E, Figure 3), on 28 February 2012, at around 100 km upstream from the mouth of the estuary. The unfiltered water was evaporated and decomposed with 15 ml of 5 M HCl, 2.1 M HNO_3, and 0.6 M HF mixing for 3 h at 130°C, then with aqua regia at 130°C during 7 h, then with 18 ml suprapur HNO_3 and 0.6 ml suprapur HF in an ultrasonic bath for 3 h, and finally with 3 ml 23 M HF and 0.5 ml 15 M HNO_3 at 130°C during 2 days. An aliquot without refractory particles was taken and centrifuged. After adding a ^{57}Fe–^{58}Fe double-spike solution, sample was purified twice with an AG-MP1 anionic resin (100–200 mesh). The blank was 0.25 ng ($n = 1$). As the total Fe content of the Sepik River sample was 218 μg (concentration of 3.9 μM), thus the blank was negligible (~0.00% of the sample content).

3.3.3. Bottom Sediments

Two samples of sediments were retrieved with a giant piston corer close to the Southern Papua New Guinea coast in the Coral Sea during the 2005 MD148 IMAGES XIII PECTEN cruise in 2005 (Figure 3) [*Tachikawa et al*., 2011], downstream the Fly river. One sample (MD05-2939) was taken at the surface of a core sampled at 9°52′S 145°45′E and beginning at 1677 m depth, and a second (MD97-2134) was taken from 4 to 5 cm below the surface of a core sampled at 9°54′S 144°39′E and beginning at 70 m depth. These samples are used to represent sediment at the sediment/seawater interface. These sediment samples were first dissolved with 5 ml of an acid mixture (HCl 6 M, HNO_3 2.3 M, HF 0.8 M) at 130°C during 3 h. After evaporation, they were mixed with 12 ml of another acid mixture (HNO_3 10 M, HF 4.5 M, HCl 1.4 M). Then, they were heated at 180°C for 2 h in a microwave oven (Mars System 5, CEM®). The total dissolution of sediments was achieved with 1 ml suprapur $HClO_4$ at 120°C during 2 days. After adding the ^{57}Fe–^{58}Fe double-spike solution, the samples were purified twice with an AG-MP1 anionic resin (100–200 mesh). Average recovery of the purification step with this resin was 103 ± 14% (2SD, $n = 41$). The blank was 16.6 ± 24.1 ng (2SD, $n = 3$) or 0.11% of sample content.

3.3.4. Rabaul Volcano Water

Surface coastal seawater at the foot of the Rabaul volcano in the East of the New Britain Island (4°14′25″S, 152°11′45″E, Figure 3) was sampled a few hundred meters from shore, where numerous small streams were flowing along the flanks of the volcanoes, delivering their erosion products to the coastal water. One sample was taken from the front of a pirogue into an acid-cleaned polyethylene bottle, just after the EUCFe cruise (2 October 2006). The unfiltered sample was acidified and then evaporated in a clean lab, and the residue was digested with 1.4 ml of aqua regia at 80°C during 1 day. An aliquot was analyzed to determine the Fe content on the ICPMS Element (Thermo Scientific®). Then, a double-spike solution of ^{57}Fe–^{58}Fe was added. Finally, the sample was purified twice with an AG1-X4 anionic resin (200–400 mesh). The blank of 1.7 ng ($n = 1$) was negligible compared to the total Fe concentration of the Rabaul water of 5.25 μM.

3.4. Isotopic Analysis

The procedure for the measurements of Fe isotopic compositions ($\delta^{56}Fe$), general performance, and validation steps were detailed in *Lacan et al*. [2010]. The Fe isotopic composition was measured with the Multi-Collector Inductively Coupled Plasma Mass Spectrometer (MC–ICPMS) Neptune (Thermo Scientific®) coupled with a desolvating nebulizer system (ESI Apex–Q® or ESI Apex-HF®). The isotopic composition of DFe was been measured at the *Observatoire Midi-Pyrénées* (OMP, Toulouse, France), while that of PFe was measured at OMP and at the *Laboratoire des Sciences du Climat et de l'Environnement* (LSCE, Gif-sur-Yvette, France).

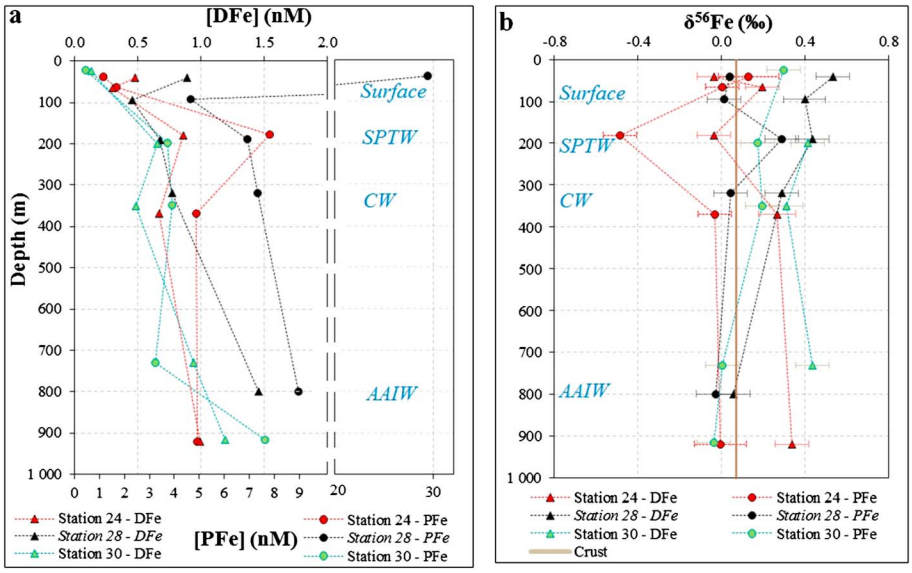

Figure 4. Profiles of (a) dissolved (triangles, upper axis) and particulate (circles, lower axis) Fe concentrations in nM (nmol.kg-1) and (b) dissolved (triangles) and particulate (circles) Fe isotopic composition in ‰ relative to IRMM-014. In each figure, green profiles are for station 30 in a Vitiaz Strait, black profiles for station 28 close to Papua New Guinea coast downstream the Sepik river, and red profiles for Station 24 close to New Ireland coast. In Figure 4a, the error bars are smaller than the symbols. The water masses corresponding to sample depths are specified in blue. Surface is for surface waters, SPTW is for Southern Pacific Tropical Waters, CW is for Central Water and AAIW is for AntArctic Intermediate Water. In Figure 4b, the vertical brown line indicates the crustal value (0.07 ± 0.02‰) [*Poitrasson*, 2006].

Mass bias was corrected with the ^{57}Fe–^{58}Fe double spike. The δ^{56}Fe values were calculated relative to the average of IRMM-14 measurements bracketing each sample. Repeated analyses of an in house hematite standard [*Poitrasson and Freydier*, 2005] provided an external reproducibility of the MC–ICPMS measurement of ± 0.07‰ (2SD, $n = 319$). Measurement uncertainty was also obtained by different kinds of replicates (sampling, chemical procedures, measurement replicates, etc.). All these replicates provide a reproducibility of ± 0.06‰ (2SD, $n = 82$). The reproducibility estimated from replicates was better than the external precision. In general, we consider that the external precision best characterizes our measurement uncertainty. When the internal precision ($2SE = 2SD/\sqrt{n}$) of a given sample is greater than the external precision, we take it as the sample measurement uncertainty.

Concerning concentrations of particulate and dissolved Fe, the double spike method provides a precise and accurate determination [*Lacan et al.*, 2010]. All replicates provide a mean uncertainty of 2.0% (2SD, $n = 110$).

4. Results and Discussion

4.1. Seawater Iron Concentrations

Dissolved and particulate Fe concentrations (Table 2) are plotted in Figure 4a (triangle symbols for DFe and circle symbols for PFe). Dissolved Fe concentrations ranged from 0.13 to 1.46 nM (Figure 4a). Particulate Fe concentrations ranged from 0.44 to 29.45 nM (Figure 4a). This range of DFe concentrations has generally been observed in other coastal areas [*Turner and Hunter*, 2001; *Mackey et al.*, 2002; *Obata et al.*, 2008; *Slemons et al.*, 2010]. Data of PFe concentrations are very scarce in the equatorial Pacific, so there are only few comparisons. Our data of PFe concentrations are comparable to data of total dissolvable Fe measured by *Mackey et al.* [2002] in the Bismarck Sea. *Slemons et al.* [2010, 2012] measured the DFe and PFe concentrations with another method at the same stations during the same cruise. All data are of the same order of magnitude and similar range.

The lowest concentrations of DFe and PFe were located in the surface layer (in general corresponding to the chlorophyll maximum) where the biological uptake depletes the concentration of the bioavailable Fe; an exception was downstream from the Sepik River at station 28, where the DFe concentration was 0.89 nM and PFe concentration was 29.5 nM, the highest values in surface waters. In this study, the biological uptake will

not be discussed because this area is strongly impacted by lithogenic inputs. Around 200 m, at the depth of the New Guinea and New Ireland Coastal Undercurrents, there was a sharp concentration increase, notably visible in Vitiaz Strait (Station 30) and along New Ireland (Station 24). Dissolved Fe and particulate Fe concentrations increased close to the bottom. Particulate Fe proportions (relative to total Fe) were large in all samples with an average of 86% PFe and a maximum of 97% at station 28 at 40 m depth.

4.2. Seawater Iron Isotopic Compositions

Dissolved δ^{56}Fe (δ^{56}DFe) and particulate δ^{56}Fe (δ^{56}PFe) for all stations are reported in Table 2 and are plotted in Figure 4b. The isotopic signatures of DFe ranged from −0.03 to 0.53‰. Few studies have investigated the isotopic composition of DFe in the marine environment. The δ^{56}DFe values presented here are in the same order of magnitude as those previously published from other oceanic areas [*De Jong et al*., 2007; *Lacan et al*., 2008; *John and Adkins*, 2012; *John et al*., 2012; *Staubwasser et al*., 2013]. The isotopic signature of PFe ranged from −0.49 to 0.34‰. The only points of comparison are the *Staubwasser et al*. [2013] data from the Baltic Sea where they found values ranging from −0.61 to −0.09‰.

From the surface down to 200 m depth, the δ^{56}DFe along Papua New Guinea (Figure 4b, green and black triangles) are positive (from 0.29 to 0.45‰), whereas those along the New Ireland from −0.03 to 0.20‰ (Figure 4b, red triangles) are close to the crust value (0.07 ± 0.02‰) [*Poitrasson*, 2006]. At 200 m depth, profiles of δ^{56}PFe show the largest variations, from −0.49‰ along New Ireland (station 24) to 0.29‰ along Papua New Guinea. At around 350 m depth, all δ^{56}DFe are similar with a mean value of 0.29 ± 0.04‰ (2SD, $n = 3$), and then toward the bottom, δ^{56}DFe are slightly different. From 700 m to 950 m, the δ^{56}PFe values are homogeneous and slightly lighter than the crust value, with a mean value of −0.02 ± 0.03‰ (2SD, $n = 4$).

4.3. Signatures of the Potential Fe Sources

The measured signatures of potential Fe sources to the ocean are reported in Table 3.

4.3.1. Continental Runoff

The Sepik River displayed a total Fe isotopic composition of 0.06 ± 0.06‰ (2SD, $n = 2$). The unfiltered coastal seawater sampled at the foot of the Rabaul Volcano (New Britain) displayed the same isotopic signature 0.06 ± 0.03‰ (2SD, $n = 2$). These are indistinguishable from the crustal value, δ^{56}Fe = 0.07 ± 0.02‰, and of the isotopic composition of the bulk Fe released to the oceans by large intertropical rivers like the Amazon [*Poitrasson et al*., 2014]. In both the Sepik River and Rabaul Volcano cases, particulate Fe was clearly the predominant fraction. These results suggest that runoff (whereas diffuse within small streams or within large rivers) carries PFe characterized by a crustal signature, predominantly reflecting the erosion of lithogenic iron [see also *Poitrasson et al*., 2008, 2014].

4.3.1.1. Dusts

Until now, atmospheric dusts were thought to have the same isotopic signature as of the crust [*Beard et al*., 2003b; *Waeles et al*., 2007; *Radic et al*., 2011]. However, these previous studies have focused on continental aerosols and gave values ranging from −0.03 to 0.24‰ with a mean of 0.1‰, i.e., close to the crustal value [*Beard et al*., 2003a; *Fantle and DePaolo*, 2004; *de Jong et al*., 2007; *Waeles et al*., 2007; *Flament et al*., 2008; *Majestic et al*., 2009a, 2009b]. In our study, marine aerosols were isotopically enriched in heavy isotopes, from 0.27 ± 0.15‰ to 0.38 ± 0.08‰. Thus, in the Bismarck Sea the "source" aerosol signature appears to be heavier than the crustal value, on average +0.33 ± 0.11‰ (2SD, $n = 3$).

This isotopic signature is heavier than that of the crust [*Poitrasson*, 2006]. Thus, marine aerosols sampled in this study did not appear to be continental dust simply being transported offshore. Such a heavy value may reflect the impact of various transformations that aerosols undergo during transport, such as photochemical reactions and leaching. Around the Bismarck Sea, there are many active volcanoes. There are no literature data for δ^{56}Fe of volcanic ash; nevertheless, their signatures should be the same as basalt or river runoff, which are the same as crust [*Poitrasson*, 2006; *Craddock et al*., 2013; *Teng et al*., 2013]. Volcanic ash probably does not explain the heavy signal measured in our samples. These heavy Fe isotopic values (Table 3) may represent elsewhere anthropogenic pollution. They are indeed in the high end of the Fe isotopic signature range of this potential source, between −0.18 and 0.34‰ [*Flament et al*., 2008; *Majestic et al*., 2009a, 2009b]. However, it is unlikely that they reveal Fe signature of anthropogenic emissions because of the weak demography of the surroundings lands (such as Papua New Guinea), the Bismarck Sea is weakly impacted by anthropogenic pollution, as most of the equatorial Pacific [*Brunskill*, 2004]. Isotopic fractionation during

Table 3. Locations, Depths, Sampling Date and Associated Cruise, Fe Concentration, and Isotopic Composition (‰) of Fe in Oceanic Dusts, in the Sepik River (Total Fe), in Sediments, and in Coastal Seawater Influenced by Runoff at the Foot of the Rabaul Volcano[a]

Samples	Location	Sampling Date	Depth		Fe Concentration	δ^{56}Fe (‰)	2SE (‰)
DUSTS					ng(Fe)/m^3		
A259	from 01.48°N, 167.31°E to 01.06°N, 164.59°E	EUCFe, 16–17/09/2006			0.38	0.27	0.15
A266	from 02.32°S, 153.56°E to 01.18°N, 146.34°E	EUCFe, 23–25/09/2006			5.56	0.35	0.07
A269	from 01.18°N, 146.33°E to 03.21°S, 143.52°E	EUCFe, 26–28/09/2006			0.54	0.38	0.08
					µmol(Fe)/L		
Sepik River	4.03°S, 144.04°E	28 February 2012	Surface	a, 1	124.6	0.07	0.07
				a, 2		0.09	0.07
				b, 1		0.04	0.07
				b, 2		0.04	0.07
				Mean		*0.06*	
Rabaul Water	4.12°S, 152.1°E	EUCFe, 2 October 2006	Surface	1	5.25	0.08	0.07
				2		0.06	0.07
				Mean		*0.07*	
Bottom Sediments					mg(Fe)/g		
MD05-2939 (core surface)	9.52°S, 145.45°E	PECTEN, 2003	1667 m	1	28.67	0.16	0.07
				2		0.10	0.07
				Mean		*0.13*	
MD97-2134 (4–5 cm of the core top))	9.54°S, 144.39°E	PECTEN, 2005	70 m	1	59.33	0.15	0.07
				2		0.13	0.07
				Mean		*0.14*	

[a]The Fe concentration is expressed in ng of Fe per m^3 of filtered air for dusts, in µmol of Fe per liter of sampled waters for Sepik River and Rabaul water, in mg of Fe per g of sampled sediments. The 2SE is the internal precision of each isotopic composition measurement. The measurement uncertainty is ±0.07‰ (2SD) or the 2SE when 2SE is larger than 0.08‰. Replicate codes (a, b, c, 1, 2, 3) as in Table 2.

aerosol transport seems the most likely hypothesis, although we cannot provide a precise mechanism explaining these observations at this stage.

4.3.1.2. Sediments

Two surface sediment samples from the southern margin of Papua New Guinea were measured in this study (see Figure 3). They were sampled from water depths of 1667 m and 70 m. The isotopic composition of both are indistinguishable, with a mean value of 0.14 ± 0.07‰ (2SD, $n = 2$). This signature is heavier than those of oceanic sediments found in previous studies (from −0.16 ± 0.07‰ to 0.1 ± 0.06‰ 2SD) [*Fantle and DePaolo*, 2004; *Severmann et al*., 2006; *Staubwasser et al*., 2006] and similar to the value obtained by *Murray et al*. [2010] downstream the Papua New Guinea, between −0.088 and + 0.164‰. In our study area, *Wu et al*. [2013] indicate that Fe-enriched sediments are mostly derived from fluvial inputs of Papua New Guinea, with nearly negligible impact from eolian dust. Therefore, we expected that the sediment signature would have been the same as measured for runoff (Sepik River and seawater sampled at the foot of the Rabaul Volcano), i.e., the crustal signature. Albeit slightly heavier, it is the same within uncertainties.

Therefore, Fe isotopic compositions do not allow distinguishing sedimentary sources from the riverine inputs in the Bismarck Sea. This is not surprising since the particulate Fe found in the sediments is mostly originating from the erosion of Papua New Guinea and transported to the shelf (and subsequently slope) through runoff [*Wu et al*., 2013]. However, the aerosols signature is clearly distinct and heavier from the other sources.

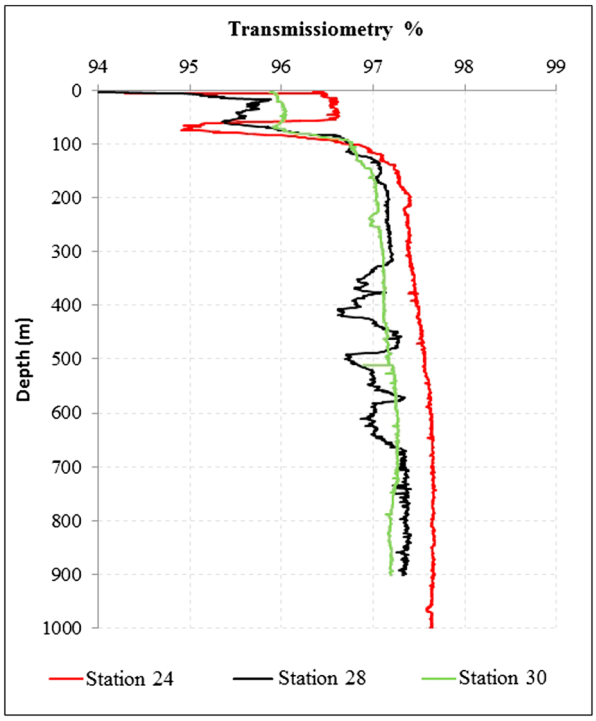

Figure 5. Profiles of transmissiometry (%). Conductivity, temperature, and depth (CTD) data.

4.4. Iron Enrichments of Water Masses in the Western Equatorial Pacific

Previous works have shown that the western equatorial Pacific is a major source area of micronutrients, and notably Fe, to the HNLC area of the equatorial Pacific via the EUC [*Sholkovitz et al.*, 1999; *Lacan and Jeandel*, 2001; *Mackey et al.*, 2002; *Slemons et al.*, 2010]. A notable feature concerning the distribution of Fe between its dissolved and particulate fractions is the overwhelming predominance of the particulate fraction (Figure 4a). In these coastal stations, the particulate fraction accounted for 86% of the total Fe budget when considering the whole water column. This means that Fe inputs are mainly in the particulate form in this area. Our samplings allow to study the Fe enrichment of four water masses (Figure 4): (i) the surface waters at station 28, (ii) the South Pacific Tropical Water (SPTW) around 200 m carried by the New Guinea Coastal Undercurrent (NGCU) and the New Ireland Coastal Undercurrent (NICU), (iii) the Central Water around 300 m also carried by NGCU, and (iv) the deeper Antarctic Intermediate Water located around 800 m.

4.4.1. Surface Seawater Enrichments

At station 28 (located around 30 km downstream from the Sepik River, Figure 3), a strong enrichment of Fe was observed in the surface waters in both the dissolved and particulate fractions (40 m, [DFe] = 0.89nM and [PFe] = 29.5 nM) compared to the upstream station in the Vitiaz Strait (station 30, 25 m, [DFe] = 0.13nM and [PFe] = 0.44 nM, Figures 2 and 3). The enrichment is very much larger in the particle fraction. The latter display the highest PFe concentration measured in the present study. Particulate Fe in this sample amounts to 97% of the total Fe. Therefore, the source of this enrichment can be considered to be mainly in the particulate form and the isotopic signal of the seawater particles, 0.04 ± 0.07‰ (station 28, 40 m, Figure 4), likely reflects directly that of the source.

Different authors have shown that atmospheric dust deposition is not sufficient to explain the strong Fe inputs to surface seawater. They concluded that this input is negligible compared to the fluvial inputs to the Bismarck Sea [*Slemons et al.*, 2010; *Wu et al.*, 2013]. Assuming that no process has fractionated particulate Fe in surface waters, our isotopic results confirm their conclusions since aerosol samples from this area (sample A269) displayed a Fe signature of 0.38 ± 0.08‰ (Table 3), which is significantly different from the particulate δ^{56}Fe value in surface waters (0.04 ± 0.07‰).

Slemons et al. [2010] and *Radic et al.* [2011] suggested that the main source of the Fe maximum at station 28 was from riverine discharge. Accordingly, the plume of Sepik discharge was visible to the naked eye during the cruise (see also the very low transmissiometry at the surface in Figure 5). The Sepik River iron isotope signature measured here had a value of 0.06 ± 0.06‰ (2SD, $n = 4$), indistinguishable from the particulate δ^{56}Fe value in surface waters (0.04 ± 0.03‰, 2SD). This suggests that lithogenic particles eroded from Papua New Guinea and transported by the Sepik River is probably the main source of particulate Fe in surface waters of station 28. Contributions from other smaller rivers and more generally runoff all along the coast from the Vitiaz Strait to station 28 may also contribute to this enrichment.

At station 30, located in Vitiaz Strait, the isotopic composition of PFe was 0.30 ± 0.07‰, with a concentration of 0.44 nM (Table 2 and Figure 4b). In this area, the particles have the same isotopic signature than that of aerosols sampled in the Bismarck Sea (0. 36 ± 0.04‰, 2SD, $n = 2$, Table 3). Therefore, aerosols may contribute

here to the surface PFe content. However, given the PFe concentration (0.44 nM) which was much lower than the PFe concentration in surface seawater at station 28 (29.45 nM), this potential aerosol contribution does not seem significant at the scale of the Bismarck Sea.

4.4.2. Enrichments of South Pacific Tropical Water

The South Pacific Tropical Water (SPTW) flows through the Coral Sea and the Solomon Sea and enters in the Bismarck Sea by two flows. The first enters in the Bismarck Sea via the NGCU (Figure 2), through Vitiaz Strait (station 30, 200 m) and flows along the North East coast of Papua New Guinea (sampled at Station 28, 190 m). The second enters the Bismarck Sea through St George channel or joins the equator directly via the NICU which flows along the North East coast of New Ireland (station 24, 180 m).

In Vitiaz Strait, at the depth of the NGCU, DFe and PFe concentrations are already high (0.65 and 3.72 nM, respectively) compared to typical open ocean values (Figure 4a). The SPTW has probably already been enriched upstream, in the Solomon and Coral seas. The positive isotopic composition measured in the Vitiaz Strait (δ^{56}PFe = 0.17 ± 0.07‰ and δ^{56}DFe = 0.41 ± 0.07‰) likely reflect those enrichments. This hypothesis is supported by Nd isotope data suggesting the occurrence of lithogenic enrichment in this water mass in those seas [*Grenier et al*., 2011].

After flowing through the Vitiaz Strait (station 30) and along the Papua New Guinea coast, the SPTW reaches station 28. There the concentration of PFe increases by 86% (to 6.9 nM, Figure 4a) between the two stations, while the concentration of DFe remains almost constant (increase of 4%). The particulate fraction is again predominant (91%). Inputs of Fe have therefore probably taken place primarily in the particulate form. The Fe signature of PFe at station 28 was δ^{56}PFe = 0.29 ± 0.07‰. Although this value is slightly different from that found at station 30 (0.17 ± 0.07‰, Figure 4a), it is very close and can be considered similar. This suggests that the source of PFe enriching this water mass along Papua New Guinea is isotopically similar to that enriching the water mass upstream in the Solomon and Coral Seas. On average, this δ^{56}Fe value is 0.23‰. The sources with similar heavy isotopic signatures are the sediments (0.14 ± 0.07‰, Table 3) and the aerosols (0.33 ± 0.11‰, Table 3). Runoff waters, with their isotopic signal similar to that of the crust (0.06 and 0.07‰ for the Sepik and Rabaul waters, respectively, Table 3), seem to be slightly too light to explain the signal measured in the SPTW. Given the depth of the SPTW flows (~200 m), it is unlikely that aerosols would constitute a significant source only at this depth, but not in the rest of the water column (where for instance at station 28 all PFe display a crustal like signature). Therefore, Fe isotopes suggest that sediment resuspension is the most likely source responsible for the PFe enrichments observed in the STPW. These results confirm the conclusions of *Slemons et al*. [2010], supported by studies of remineralization rates of organic carbon [*Burns et al*., 2008] and the high oxygen levels of this area (G. J. Brunskill, unpublished data, 1996), which suggest that the main source of Fe along Papua New Guinea would be the resuspension of sediments whose fluxes would be larger than those induced by diagenetic remobilization.

The other branch of the SPTW flows in the NICU, along the Northwest coast of New Ireland, where it was sampled at station 24 at 180 m. Its particulate iron content is also very high ([PFe] = 7.81 nM, Table 2 and Figure 4a), comparable to that found at station 28 (6.9 nM). But unlike other stations (28 and 30), the high PFe concentrations constitute a sharp vertical maximum (the sample below being much less concentrated). Particulate Fe is again the predominant fraction (90%), suggesting inputs mostly in the particulate form. The striking feature of this sample is its negative signal, δ^{56}PFe = −0.48 ± 0.07‰ (Table 2 and Figure 4b), that is very different from those found along the Papua New Guinea coast (Stations 30 and 28). This negative signal suggests a different source for PFe. This difference in the isotopic composition of PFe is the only geochemical parameter measured during the cruise at station 24 that allows identification of a different nature of the Fe source in the NICU. Indeed, the data for Rare Earth Elements (REE), aluminum and manganese, did not suggest different sources between these two areas [*Slemons et al*., 2010, 2012; *Grenier et al*., 2013]. This region, also known as Manus Basin, is rich in submarine hydrothermal activities [*Both et al*., 1986; *Auzende et al*., 1996, 2000], and station 24 is surrounded by active vent sites such New World Seamount (2°8′S, 152°53′E), Luise Harbor (3°11′S, 152°65′E), Edisson Seamount (3.31°S, 152.58°E), or Waramung (4°08′S, 153°667′E) (www.interridge.org). The Fe isotopic signature of particles measured in buoyant hydrothermal plumes range from −0.70 ± 0.1 to −0.11 ± 0.07‰ [*Severmann et al*., 2004; *Bennett et al*., 2009]. Our sample from the NICU falls within this range. Therefore, the active hydrothermal activity of the basin could explain this negative δ^{56}PFe value. Although a contribution of lithogenic sediment resuspension cannot be completely ruled out, it is likely minor compared to

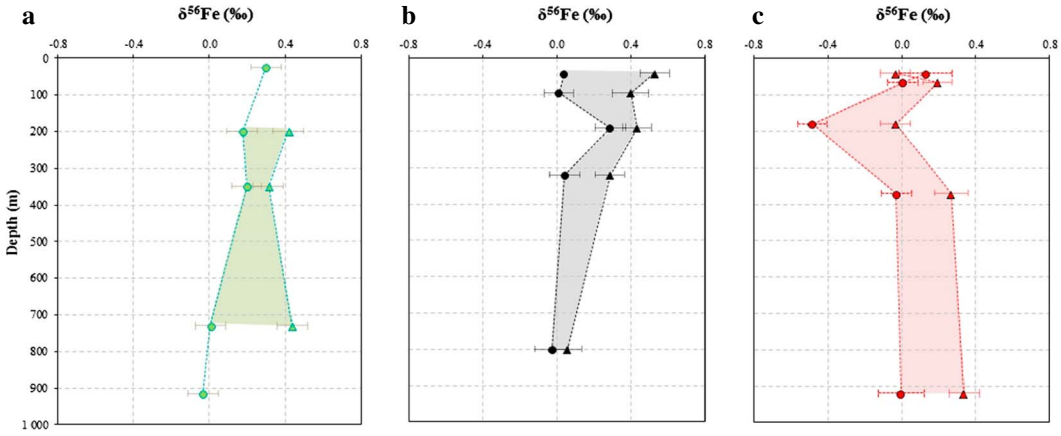

Figure 6. Profiles of dissolved (triangles) and particulate (circles) Fe isotopic composition in ‰ of (a) station 30 in a Vitiaz Strait, (b) station 28 close to the Papua New Guinea coast downstream the Sepik river, and (c) station 24 close to New Ireland coast. The colored area represents the difference between the δ^{56}DFe and the δ^{56}PFe. The dissolved Fe is almost systemically heavier than the particulate Fe.

hydrothermal activity given the slightly heavy signature of the sediments in the studied area (δ^{56}Fe = 0.14 ± 0.07‰, Table 3).

4.4.3. Central Water Enrichments

At station 28, in the Central Water at 320 m, the concentration of PFe continues to increase (7.3 nM, Figure 4a). The transmissiometry profile (Figure 5) shows an important nepheloid layer in this station with the lowest transmissiometry values between 300 and 650 m depth. Several previous studies had indicated that the continental particulate matter discharged through runoff, notably by the Sepik River, is effectively transported across the shelf and slope to depths as deep as 2000 m, within hyperpycnal flows [*Kineke et al.*, 2000; *Walsh and Nittrouer*, 2003; *Kuehl*, 2004]. This could therefore explain the large PFe concentration in the Central Water. This would be consistent with the isotopic signature of these particles, δ^{56}Fe = 0.04 ± 0.07‰, which are identical within uncertainties to the Sepik signature (0.06 ± 0.05‰, 2SD, n = 4, Table 3). A contribution of sediment resuspension during transport of the Central Water from Vitiaz Strait to station 28 may also occur, given that the signature of the sediments (0.14 ± 0.07‰, 2SD, *n* = 4, Table 3) is also identical within uncertainties to that of PFe in the Central Water.

4.4.4. Deepest Enrichments

For the deepest samples of the three profiles (799 to 920 m), in the AAIW, the particulate fraction was again predominant: 86, 82, and 83% of total Fe for respectively stations 30, 28, and 24. As for the other depths, this suggests that Fe inputs into these waters occur mainly in the particulate phase. In these three stations, the isotope composition of particulate Fe tends toward a value slightly lower than the crustal value, from −0.03 ± 0.07‰ to 0.00 ± 0.12‰ (Table 2). This suggests that in addition to continental particulate matter discharged through runoff and transported to depth (characterized by signatures of 0.06 to 0.07 ± 0.07‰), and/or to sediment resuspension (0.14 ± 0.07‰), particles of hydrothermal origin may also contribute to enrich the AAIW.

4.5. Exchange Processes From Particulate to Dissolved Fraction

An important feature concerning the difference between the isotopic compositions of dissolved Fe and particulate Fe is that in nearly all samples from the three stations of this study (except one at the surface of station 24), the δ^{56}DFe is heavier than the δ^{56}PFe (Figure 6). This is observed in station 24 (with its negative signal at 200 m, Figure 4b) and along the coast of Papua New Guinea (with positive signal at the same depth, Figure 4b). Furthermore this difference is rather similar for all samples. This suggests a link between both phases, associated to a systematic isotopic fractionation. Three hypotheses are examined in the following to explain this observation.

1. This difference is the result of a kinetic fractionation during the release of DFe from a partial dissolution of particulate iron. This is not possible because kinetic fractionation would produce a DFe lighter than PFe [*Urey*, 1947], which is not what we observe (Figure 4b).

2. Conversely, the difference is the result of a kinetic fractionation during the formation of PFe from dissolved iron precipitation. This would be consistent with PFe being isotopically lighter than DFe but would imply that most PFe found in our samples originates from dissolved Fe. As discussed above, PFe is the main pool in all our samples, 86% of the total seawater iron on average, with concentrations of the order of 5nM, while DFe concentrations are on the order of 0.5 nM. Particulate Fe tends to be predominant in the potential atmospheric and riverine sources [*De Baar and De Jong*, 2001]. For instance, the particulate fraction range from 50 to 99% of total Fe pool in the worldwide rivers [*Dupre et al*., 1996; *Gaillardet et al*., 1997; Mulholland et al., Insights on iron sources and pathways in the Amazon River privided by isotopic and spectroscopic studies, *Geochimica Et Cosmochimica Acta*, in revision, 2014] and after flocculation processes in estuaries, the riverine Fe input to oceans are dominantly in the particulate form [*Beard et al*., 2003a; *Fantle and DePaolo*, 2004]. This hypothesis is therefore very unlikely. Moreover, a similar isotopic difference for all samples, implies that either (i) the PFe pool is the instantaneous product of the reaction, which is highly unlikely because it would require an unrealistically high and permanent DFe source to sustain the reaction in all the samples, or (ii) in all samples a similar proportion of the DFe pool has been transferred into the PFe pool, which would also be an extraordinary coincidence. Furthermore, previous studies have shown that in this area little dissolved Fe was released from sediments compared to a significant rate of sediment resuspension [*Slemons et al*., 2010; *Burns et al*., 2008]. For these reasons, the concentration partitions, and isotopic differences, this hypothesis can be ruled out. On the contrary, if there is a net transfer from one pool to another, the above arguments strongly suggest that it occurs from PFe to DFe.
3. The isotopic difference is the result of an equilibrium fractionation between PFe and DFe. This third hypothesis is consistent with both the concentration and the isotope partitioning in our study. Unlike previous hypotheses, it appears as the only plausible explanation. It constitutes strong evidence that there is continuous exchange of iron between the two phases. Such exchange was also initially been proposed for thorium and protactinium, the so called "reversible scavenging", later for Rare Earth Elements [*Nozaki and Alibo*, 2003], then neodymium, the so called "boundary exchange" [*Lacan and Jeandel*, 2005], and more recently for Cu [*Little et al*., 2013].

The equilibrium isotopic fractionation between PFe and DFe can be quantified by calculating the isotopic difference between both phases:

$$\Delta^{56}\mathrm{Fe}_{\mathrm{DFe-PFe}} = \delta^{56}\mathrm{DFe} - \delta^{56}\mathrm{PFe} \quad (2)$$

Extreme values were found in surface samples, $\Delta^{56}\mathrm{Fe}_{\mathrm{DFe\,-\,PFe}} = -0.17$ and 0.49‰, at 40 m at station 24 and 28, respectively, in the chlorophyll maxima. Those extrema may be explained by biological processes and/or direct dissolved Fe input from the Sepik River at station 28. We therefore exclude them from the following discussion.

Averaging this difference for all other samples (for which both DFe and PFe isotope data have been measured), we find that $\Delta^{56}\mathrm{Fe}_{\mathrm{DFe\,-\,PFe}} = +0.27 \pm 0.25$‰ (2SD, $n = 11$)

As mentioned above, given the wide predominance of the particulate Fe pool in both the sources and seawater, the net result of these exchanges between PFe and DFe is most likely a net flux from PFe to DFe. In the water column, processes leading to a release of DFe from suspended particles can be reductive dissolution by bacteria, or a nonreductive release of DFe, as proposed by *Radic et al*. [2011]. The reductive dissolution (involving reduction of Fe^{III} to Fe^{II}) would produce lighter DFe [*Beard et al*., 2003b; *Severmann et al*., 2006, 2010]. Therefore, the data presented in this work confirm those presented by *Radic et al*. [2011] from station 28 only. They suggest that in all our samples, except for the two surface samples excluded as discussed above, dissolved Fe is released from particulate Fe through nonreductive processes. This should be understood as the net result of exchange processes between both phases; i.e., there may be fluxes in both directions, from PFe to DFe and from DFe to PFe, but the net result of those is a net flux from PFe to DFe, without net iron reduction. Similar observations suggest similar processes of DFe release along the South African margin [*Homoky et al*., 2013].

The precise underlying processes cannot be determined from the present study. A better characterization of the various Fe phases and in vitro experiments could help in that respect.

4.6. Flux of Fe Along the Papua New Guinea

The Fe fluxes involved in the evolution of the iron concentrations as the water masses flow along the slope of Papua New Guinea can be estimated using a simple box model. The model will be applied to the Central Water, because a significant DFe concentration increase is observed in this water mass. The system is assumed to be in steady state. The potential flows from New Ireland and St George channel toward station 28 are ignored given that their water mass transport is ~10 times lower than that in the NGCU [*Grenier et al*., 2014]. Therefore, all waters found at station 28 are assumed to flow from the Vitiaz strait, hence from station 30. The Central water is transported by the NGCU that flows with a velocity ranging from 0.2 to 1 m s^{-1} [*Wyrtki and Kilonsky*, 1984; *Rowe et al*., 2000; *Slemons et al*., 2010]. The suspended particles (sampled in the present study) sink with a typical velocity of around 1000 m yr^{-1} [*Stemmann et al*., 2004]. This is very low compared to the current velocity so inputs and outputs of particles into the box are ignored. This would still be true even if assuming a much larger sinking velocities that could occur in coastal areas (e.g. of the order of several hundred meters per day, *Berelson* [2001]).

For particulate Fe, fluxes entering the box are (1) the PFe carried within the seawater at station 30, W $[PFe]_{30}$, where W is the water mass transport, 3.4 Sv [*Lindstrom et al*., 1987, 1990; *Butt and Lindstrom*, 1994; *Melet et al*., 2010; *Cravatte et al*., 2011; *Grenier et al*., 2014], and (2) PFe provided by external sources (e.g., sediments for SPTW and continental particulate matter discharged through runoff and transmitted to depth for Central Water, cf. above), $F_{input\ PFe}$. The fluxes exiting the box are (1) the PFe carried within the seawater at station 28, W $[PFe]_{28}$, and (2) the net flux from PFe to DFe, $F_{dissolution/desorption}$, resulting from exchanges between particulate and dissolved fraction (precipitation/dissolution, adsorption/desorption), and in particular, from nonreductive release of DFe from particles, as discussed in section 4.5. For dissolved Fe, entering and exiting fluxes are defined similarly.

At steady state, mass balance implies that the fluxes entering and exiting the box are equal, which leads to

$$W \cdot [PFe]_{30} + F_{input\ PFe} = W \cdot [PFe]_{28} + F_{dissolution/desorption} \quad (3)$$

$$W \cdot [DFe]_{30} + F_{input\ DFe} + F_{dissolution/desorption} = W \cdot [DFe]_{28} \quad (4)$$

As discussed in section 4.4, the particulate fraction widely predominates external inputs. Hence, we will neglect in the following $F_{input\ DFe}$. The system can be thus solved for the two remaining unknowns: $F_{input\ PFe}$ and $F_{dissolution/desorption}$.

Solving the system, the input flux of PFe into the water mass was estimated at $F_{input\ PFe} = 22\,345 \pm 641$ T(PFe) yr^{-1} (2SD). The sediment discharge of the Northwestern slope of Papua New Guinea was estimated to be 860.10^6 T yr^{-1} [*Milliman et al*., 1999]. Iron constitutes ~4 wt.% of the local volcanic rocks [*Woodhead et al*., 2010] in this area, so that the continental PFe discharge to this side of Papua New Guinea would be 34.10^6 T(PFe) yr^{-1}. Therefore, Papua New Guinea easily provides enough material to explain the observed PFe enrichments in the SPTW, as the latter represents only 0.07% of the former. The flux of DFe brought by the flux $F_{dissolution/desorption}$ was found to be 1705 ± 5 T yr^{-1} (i.e., 8% of the $F_{input\ PFe}$).

Considering that the water mass flows along the continental slope and that external PFe inputs occur through this sediment-seawater interface, we will normalize the external PFe fluxes estimated above to the slope/water mass contact area. The surface of the slope in contact with the water mass is assumed as a rectangle with a length equal to the distance between station 30 and station 28 (511 km) and with the thickness of the water mass (~100 m). This leads to a PFe flux of 21.4 ± 0.6 mmol(PFe) m^{-2} d^{-1} in the Central Water. Normalizing to the same surfaces the flux of DFe resulting from the desorption and/or dissolution of PFe leads to 1633 ± 5 μmol(DFe) m^{-2} d^{-1}. This net $F_{dissolution/desorption}$ flux would represent the nonreductive release of DFe from particles of continental origin discharged on the margin through runoff. Previous studies of the DFe release from margin sediments were conducted in areas with reducing sediments and focused on reductive Fe dissolution. In the latter studies, the DFe flux from sediments ranges from -0.2 to 568 μmol (DFe) m^{-2} d^{-1} [*Elrod et al*., 2004; *Moore et al*., 2004; *Burns et al*., 2008; *Severmann et al*., 2010]. The present results suggest that the flux resulting from the nonreductive release of DFe from continental margin particles could locally be three times as large as the DFe flux from reductive dissolution. On the other hand, for the other water masses flowing along Papua New Guinea, the SPTW, and the AAIW, the fluxes are found smaller, 60 ± 2 and 877 ± 2 μmol m^{-2} d^{-1}, or 27 and 2 times less than inputs in the Central Water, respectively.

Therefore, for the top 1000 m of the water column (the depth we sampled), averaging the values found for the three water masses, the flux associated to nonreductive release of DFe would be 857 μmol m^{-2} d^{-1}.

Contrary to reductive dissolution (which require oxygen-depleted environments to occur), nonreductive release of DFe could occur along all ocean margins, as long as erosion delivers continental particles to the shelves and slopes. If we extrapolate the above results globally (fluxes comprised between 60 and 1633 μmol m^{-2} d^{-1}), considering that the margin surface represents around 8% [*Menard and Smith*, 1966; *Elrod et al*., 2004] of the global ocean surface (8% of 3.6×10^{14}m^2), this nonreductive release could provide from 9 to 960Tg(DFe) yr^1 into the ocean, whereas previous studies estimate that reductive dissolution could bring 1.8 to 5 Tg(DFe) yr^{-1} [*Johnson et al*., 1999; *Beard et al*., 2003a; *Elrod et al*., 2004; *Moore and Braucher*, 2008] and that the dust deposition could bring 0.1 to 1.2 Tg(DFe) yr^{-1} [*Beard et al*., 2003a; *Elrod et al*., 2004; *Jickells et al*., 2005; *Waeles et al*., 2007].

This study was carried in an area of especially intense sedimentary discharge. The above extrapolation, and particularly its upper limit, could therefore be overestimated and needs to be considered cautiously. Of course, more data from diverse areas would be required to better estimate the magnitude of the nonreductive release of DFe. However, the present data set suggests it could be significant and even maybe larger than the other DFe sources documented so far (notably dusts, DFe carried by rivers, sediment reductive dissolution, and hydrothermal activity).

4.7. Residence Time

The residence time of dissolved and particulate Fe was estimated from the amount of iron in the water mass (Q_{Fe}) divided by the sum of entering fluxes or the sum of outgoing fluxes (both being equal at steady state):

$$\tau_{Fe} = \frac{Q_{Fe}}{\sum_{\text{entering} \triangleright \text{Flux}}} \quad (5)$$

The reservoir considered here is the water column from station 30 to station 28 (511 km length), 5 km wide (the mean width of the shelf [*Slemons et al*., 2010, *Kineke et al*., 2000]) and 900 m thick. The residence time is 0.68 ± 0.03 days for PFe and 1.11 ± 0.03 days for DFe. In the global ocean, the residence time of DFe ranges from 15 to 200 years [*Turner and Hunter*, 2001; *Boyd and Ellwood*, 2010]. Specifically, it has been computed to range from 70 to 200 years in the North Pacific [*Bruland et al*., 1994; *Johnson et al*., 1997] and from 5 to 200 years in other area of ocean [*Landing and Westerlund*, 1988; *Bergquist and Boyle*, 2006a, 2006b; *Boyd and Ellwood*, 2010]. In the Central Water, the DFe residence time was very much shorter. Few studies estimated the residence time of particulate iron. In Subantarctic waters, Southeast of New Zealand, the residence time of PFe was estimated to be 100 days [*Frew et al*., 2006]. Here, it was 2 orders of magnitude shorter. The difference between the DFe and PFe residence times found here compared to literature values is due to the immediate vicinity of Fe external inputs and to the strong dynamic of the area, leading to a rapid input and output of DFe and PFe from the water masses.

5. Conclusion

The Fe isotopic composition of potential iron sources to the western equatorial Pacific Ocean has been documented. Aerosols present signatures from δ^{56}Fe = 0.27 to 0.38 ± 0.08‰. In contrast to previous reports focused on continental aerosols [*Beard et al*., 2003a], these values are heavier than the crust (0.07 ± 0.02‰) [*Poitrasson*, 2006]. This heavy range likely reflects transformations that aerosols undergo during their transport after their site of origin, such as photochemical reactions and leaching. Sediment samples present a signature undistinguishable within uncertainties from that of crust, i.e., δ^{56}Fe = 0.14 ± 0.07‰, albeit slightly heavier. The Sepik river water and coastal seawater reflecting the influence of runoff at the base of the Rabaul volcano also had δ^{56}Fe values similar to that of crust, 0.06 ± 0.05‰ (2SD, $n = 4$) and 0.07 ± 0.03‰ (2SD, $n = 2$), respectively. Thus, in the Bismarck Sea, the Fe isotopic compositions do not allow distinguishing sedimentary sources from the riverine inputs. This is not surprising since the particulate Fe found in the sediments mostly originates from erosion of Papua New Guinea, and transportation to the shelf and slope, through runoff [*Wu et al*., 2013]. The aerosols signature is clearly distinct from the other sources.

The significant regional variation of PFe and DFe isotopic signature in seawater, from δ^{56}Fe = −0.49 to 0.34 ± 0.07‰ and from -0.03 to 0.53 ± 0.07‰, respectively, supports the growing interest in iron isotopes for studying oceanic biogeochemical cycles [*Lacan et al*., 2008, 2010; *John and Adkins*, 2010, 2012; *Radic et al*.,

2011]. In this work, Fe isotopes have allowed to distinguish different Fe sources. In most places, they suggest that particulate Fe enrichments (which widely dominate dissolved Fe enrichments) result from continental erosion, either through direct river inputs and subsequent particle transport across shelves and slopes or via lithogenic sediment remobilization. The fact that DFe is released along Papua New Guinea from continental particles delivered to the shelf and slope through runoff seems a robust conclusion, as it has been suggested in several previous studies [*Lacan and Jeandel*, 2001; *Mackey et al*., 2002; *Slemons et al*., 2010]. An aerosol contribution is suspected in the surface waters of the Vitiaz Strait. A sharp isotope minimum at 200 m depth along New Ireland suggests enrichment due to hydrothermal sources.

In all our samples except two surface samples potentially influenced by biological processes, a systematic positive difference was measured between δ^{56}PFe and δ^{56}DFe ($\Delta^{56}Fe_{DFe-PFe} = +0.27 \pm 0.25‰$, 2SD, $n = 11$). This and the wide predominance of PFe relative to DFe suggest (i) the occurrence of permanent exchange between dissolved and particulate Fe, associated to an equilibrium isotopic fractionation, and (ii) that these exchanges result in a net nonreductive release of DFe from PFe. Because dissolved δ^{56}Fe is heavier than particulate δ^{56}Fe, a net reduction during dissolution is unlikely. When *Radic et al*. [2011] introduced this concept, they named it "nonreductive dissolution". This term was later used by *Homoky et al*. [2013] about pore waters in South Africa. We argue here that the exact process responsible for the release of DFe is not constrained, as it could be dissolution but also desorption. Thus, we suggest that the formulation "nonreductive release of DFe" is more appropriate. We suggest that such exchanges could be the same as those proposed to describe the cycles of other particle reactive elements, Th, Pa, REE, Nd isotopes, and Cu.

Based on a simple box model, the nonreductive release would bring from 60 to 1633 μmol(DFe) m^{-2} d^{-1}. Extrapolating such values to the margin area of the global ocean would lead to a flux from 9 to 960 Tg(DFe) yr^{-1}. Compared to Fe reductive dissolution, observed in oxygen depleted areas, estimated on the global scale from 1.8 to 5 Tg(DFe) yr^{-1} [*Elrod et al*., 2004; *Moore and Braucher*, 2008] and to dust dissolution estimated from 0.1 to 1.2 Tg DFe yr^{-1} [*Jickells et al*., 2005; *Waeles et al*., 2007], the nonreductive release of DFe from erosion-born PFe could constitute a significant source of dissolved Fe on the global scale. This would significantly reduce its mean oceanic residence time and increase its global oceanic sink (assuming steady state). Such process may involve other elements. The release of dissolved species from lithogenic particles delivered to the ocean through runoff has been observed or suggested for a growing number of elements, Nd, Sr, Si, Ca, etc. [*Tachikawa et al*., 2003; *Jeandel et al*., 2011; *Jones et al*., 2012]. Understanding the underlying processes is a major and important challenge for improving our understanding of global oceanic biogeochemical cycles.

Acknowledgments

L. Shank is thanked for providing the aerosol samples. O. Yigiterhan, S. Bonnet, C. Venchiarutti, and J. Resing are thanked for their help with the seawater sampling. J. Chmeleff, F. Candaudap, and A. Lanzanova are thanked for their support with the ICP-MS. The captain and the crew of the R/V *Kilo Moana* and especially marine technicians G. Foreman and D. Fitzgerald are greatly acknowledged. We thank L. Beaufort and K. Tachikawa for giving us samples of Sepik River and sediments. The CNRS (French National Center for Scientific Research) and the University of Toulouse are thanked for supporting this study.

References

Ardelan, M. V., O. Holm-Hansen, C. D. Hewes, C. S. Reiss, N. S. Silva, H. Dulaiova, E. Steinnes, and E. Sakshaug (2010), Natural iron enrichment around the Antarctic Peninsula in the Southern Ocean, *Biogeosciences*, *7*(1), 11–25.

Auzende, J.-M., et al. (1996), Activité tectonique, magmatique et hydrothermale dans le bassin de Manus (SW Pacifique, Papouasie-Nouvelle Guinée): Campagne MANUSFLUX du Shinkai-6500, *C.R. Acad. Sci., Ser. IIa: Sci. Terre Planets*, *323*, 501–508.

Auzende, J.-M., et al. (2000), The eastern and western tips of Manus Basin (Papua, New Guinea) explored by submersible, MANAUTE cruise, *C.R. Acad. Sci., Ser. IIa, Earth Planet. Sci.*, *331*(2), 119–126.

Beard, B. L., and C. M. Johnson (2004), Fe isotope variations in the modern and ancient Earth and other planetary bodies, *Rev. Mineral. Geochem.*, *55*(1), 319–357.

Beard, B. L., C. M. Johnson, J. L. Skulan, K. H. Nealson, L. Cox, and H. Sun (2003a), Application of Fe isotopes to tracing the geochemical and biological cycling of Fe, *Chem. Geol.*, *195*(1), 87–117.

Beard, B. L., C. M. Johnson, K. L. Von Damm, and R. L. Poulson (2003b), Iron isotope constraints on Fe cycling and mass balance in oxygenated Earth oceans, *Geology*, *31*(7), 629–632.

Behrenfeld, M., A. Bale, Z. Kolber, J. Aiken, and P. Falkowski (1996), Confirmation of iron limitation of phytoplankton photosynthesis in the equatorial Pacific Ocean, *Nature*, *383*(6600), 508–511.

Bennett, S. A., O. Rouxel, K. Schmidt, D. Garbe-Schönberg, P. J. Statham, and C. R. German (2009), Iron isotope fractionation in a buoyant hydrothermal plume, 5°S Mid-Atlantic Ridge, *Geochim. Cosmochim. Acta*, *73*(19), 5619–5634.

Berelson, W. M. (2001), Particle settling rates increase with depth in the ocean, *Deep Sea Res., Part II*, *49*(1–3), 237–251, doi:10.1016/S0967-0645(01)00102-3.

Bergquist, B. A., and E. A. Boyle (2006b), Dissolved iron in the tropical and subtropical Atlantic Ocean, *Global Biogeochem. Cycles*, *20*, GB1015, doi:10.1029/2005GB002505.

Bergquist, B., and E. Boyle (2006a), Iron isotopes in the Amazon River system: Weathering and transport signatures, *Earth Planet. Sci. Lett.*, *248*(1–2), 54–68.

Blain, S., S. Bonnet, and C. Guieu (2008), Dissolved iron distribution in the tropical and sub tropical South Eastern Pacific, *Biogeosciences*, *5*(1), 269–280.

Both, R., K. Crook, B. Taylor, S. Brogan, B. Chappell, E. Frankel, L. Liu, J. Sinton, and D. Tiffin (1986), Hydrothermal chimneys and associated fauna in the Manus Back-Arc Basin, Papua New Guinea, *Eos Trans. AGU*, *67*(21), 489–490, doi:10.1029/EO067i021p00489.

Boyd, P. W., and M. J. Ellwood (2010), The biogeochemical cycle of iron in the ocean, *Nat. Geosci.*, *3*(10), 675–682.
Boyd, P. W., et al. (2007), Mesoscale iron enrichment experiments 1993–2005: Synthesis and future directions, *Science*, *315*(5812), 612–617.
Boyle, E., and W. Jenkins (2008), Hydrothermal iron in the deep western South Pacific, *Geochim. Cosmochim. Acta*, *72*(12), A107–A107.
Bruland, K. W., K. J. Orians, and J. P. Cowen (1994), Reactive trace metals in the stratified central North Pacific, *Geochim. Cosmochim. Acta*, *58*(15), 3171–3182.
Brunskill, G. J. (2004), New Guinea and its coastal seas, a testable model of wet tropical coastal processes: An introduction to Project TROPICS, *Cont. Shelf Res.*, *24*(19), 2273–2295, doi:10.1016/j.csr.2004.08.001.
Burns, K. A., G. Brunskill, D. Brinkman, and I. Zagorskis (2008), Organic carbon and nutrient fluxes to the coastal zone from the Sepik River outflow, *Cont. Shelf Res.*, *28*(2), 283–301.
Butt, J., and E. Lindstrom (1994), Currents off the east coast of New Ireland, Papua New Guinea, and their relevance to regional undercurrents in the western equatorial Pacific Ocean, *J. Geophys. Res.*, *99*(C6), 12,503–12,514, doi:10.1029/94JC00399.
Chen, J.-B., V. Busigny, J. Gaillardet, P. Louvat, and Y.-N. Wang (2014), Iron isotopes in the Seine River (France): Natural versus anthropogenic sources, *Geochim. Cosmochim. Acta*, *128*, 128–143.
Coale, K., S. Fitzwater, R. Gordon, K. Johnson, and R. Barber (1996), Control of community growth and export production by upwelled iron in the equatorial Pacific Ocean, *Nature*, *379*(6566), 621–624.
Conway, T., and S. G. John (2014), Quantification of sources of dissolved iron to the North Atlantic Ocean, *Nature*, *511*, 212–215.
Conway, T. M., A. D. Rosenberg, J. F. Adkins, and S. G. John (2013), A new method for precise determination of iron, zinc and cadmium stable isotope ratios in seawater by double-spike mass spectrometry, *Anal. Chim. Acta*, *793*, 44–52.
Craddock, P. R., J. M. Warren, and N. Dauphas (2013), Abyssal peridotites reveal the near-chondritic Fe isotopic composition of the Earth, *Earth Planet. Sci. Lett.*, *365*, 63–76, doi:10.1016/j.epsl.2013.01.011.
Cravatte, S., A. Ganachaud, Q.-P. Duong, W. S. Kessler, G. Eldin, and P. Dutrieux (2011), Observed circulation in the Solomon Sea from SADCP data, *Prog. Oceanogr.*, *88*(1–4), 116–130.
De Baar, H. J., and J. de Jong (2001), Distributions, sources and sinks of iron in seawater, *IUPAC Ser. Anal. Phys. Chem. Environ. Syst.*, *7*, 123–254.
De Jong, J., V. Schoemann, J.-L. Tison, S. Becquevort, F. Masson, D. Lannuzel, J. Petit, L. Chou, D. Weis, and N. Mattielli (2007), Precise measurement of Fe isotopes in marine samples by multi-collector inductively coupled plasma mass spectrometry (MC-ICP-MS), *Anal. Chim. Acta*, *589*(1), 105–119.
dos Santos Pinheiro, G. M., F. Poitrasson, F. Sondag, L. C. Vieira, and M. M. Pimentel (2013), Iron isotope composition of the suspended matter along depth and lateral profiles in the Amazon River and its tributaries, *J. South Am. Earth Sci.*, *44*, 35–44.
Duce, R. A., and N. W. Tindale (1991), Atmospheric transport of iron and its deposition in the ocean, *Limnol. Oceanogr.*, *36*, 8.
Dupre, B., J. Gaillardet, D. Rousseau, and C. J. Allegre (1996), Major and trace elements of river-borne material: The Congo Basin, *Geochim. Cosmochim. Acta*, *60*(8), 1301–1321, doi:10.1016/0016-7037(96)00043-9.
Elrod, V. A., W. M. Berelson, K. H. Coale, and K. S. Johnson (2004), The flux of iron from continental shelf sediments: A missing source for global budgets, *Geophys. Res. Lett.*, *31*, L12307, doi:10.1029/2004GL020216.
Escoube, R., O. Rouxel, E. Sholkovitz, and O. Donard (2009), Iron isotope systematics in estuaries: The case of North River, Massachusetts (USA), *Geochim. Cosmochim. Acta*, *73*(14), 4045–4059.
Fantle, M. S., and D. J. DePaolo (2004), Iron isotopic fractionation during continental weathering, *Earth Planet. Sci. Lett.*, *228*(3–4), 547–562.
Fine, R., R. Lukas, F. Bingham, M. Warner, and R. Gammon (1994), The Western Equatorial Pacific—A water mass crossroads, *J. Geophys. Res.*, *99*(C12), 25,063–25,080, doi:10.1029/94JC02277.
Flament, P., N. Mattielli, L. Aimoz, M. Choel, K. Deboudt, J. de Jong, J. Rimetz-Planchon, and D. Weis (2008), Iron isotopic fractionation in industrial emissions and urban aerosols, *Chemosphere*, *73*(11), 1793–1798.
Frew, R. D., D. A. Hutchins, S. Nodder, S. Sanudo-Wilhelmy, A. Tovar-Sanchez, K. Leblanc, C. E. Hare, and P. W. Boyd (2006), Particulate iron dynamics during FeCycle in subantarctic waters southeast of New Zealand, *Global Biogeochem. Cycles*, *20*, GB1S93, doi:10.1029/2005GB002558.
Gaillardet, J., B. Dupre, C. J. Allegre, and P. Negrel (1997), Chemical and physical denudation in the Amazon River basin, *Chem. Geol.*, *142*(3–4), 141–173, doi:10.1016/S0009-2541(97)00074-0.
Gordon, R. M., K. H. Coale, and K. S. Johnson (1997), Iron distributions in the equatorial Pacific: Implications for new production, *Limnol. Oceanogr.*, *42*(3), 419–431.
Grenier, M., S. Cravatte, B. Blanke, C. Menkes, A. Koch-Larrouy, F. Durand, A. Melet, and C. Jeandel (2011), From the western boundary currents to the Pacific Equatorial Undercurrent: Modeled pathways and water mass evolutions, *J. Geophys. Res.*, *116*, C12044, doi:10.1029/2011JC007477.
Grenier, M., C. Jeandel, F. Lacan, D. Vance, C. Venchiarutti, A. Cros, and S. Cravatte (2013), From the subtropics to the central equatorial Pacific Ocean: Neodymium isotopic composition and rare earth element concentration variations, *J. Geophys. Res. Oceans*, *118*, 592–618, doi:10.1029/2012JC008239.
Grenier, M., C. Jeandel, and S. Cravatte (2014), From the subtropics to the equator in the Southwest Pacific: Continental material fluxes quantified using neodymium data along modeled thermocline water pathways, *J. Geophys. Res. Oceans*, *119*, 3948–3966, doi:10.1002/2013JC009670.
Homoky, W. B., S. Severmann, R. A. Mills, P. J. Statham, and G. R. Fones (2009), Pore-fluid Fe isotopes reflect the extent of benthic Fe redox recycling: Evidence from continental shelf and deep-sea sediments, *Geology*, *37*(8), 751–754.
Homoky, W. B., S. G. John, T. M. Conway, and R. A. Mills (2013), Distinct iron isotopic signatures and supply from marine sediment dissolution, *Nat. Commun.*, *4*, 2143, doi:10.1038/ncomms3143.
Ingri, J., D. Malinovsky, I. Rodushkin, D. C. Baxter, A. Widerlund, P. Andersson, Ö. Gustafsson, W. Forsling, and B. Öhlander (2006), Iron isotope fractionation in river colloidal matter, *Earth Planet. Sci. Lett.*, *245*(3–4), 792–798.
Jeandel, C., B. Peucker-Ehrenbrink, M. T. Jones, C. R. Pearce, E. H. Oelkers, Y. Godderis, F. Lacan, O. Aumont, and T. Arsouze (2011), Ocean margins: The missing term in oceanic element budgets?, *Eos Trans. AGU*, *92*(26), 217–218, doi:10.1029/2011EO260001.
Jickells, T. D., et al. (2005), Global iron connections between desert dust, Ocean Biogeochemistry, and Climate, *Science*, *308*(5718), 67–71.
John, S. G., and J. Adkins (2012), The vertical distribution of iron stable isotopes in the North Atlantic near Bermuda, *Global Biogeochem. Cycles*, *26*, GB2034, doi:10.1029/2011GB004043.
John, S. G., J. Mendez, J. Moffett, and J. Adkins (2012), The flux of iron and iron isotopes from San Pedro Basin sediments, *Geochim. Cosmochim. Acta*, *93*, 14–29.
John, S., and J. Adkins (2010), Analysis of dissolved iron isotopes in seawater, *Mar. Chem.*, *119*(1–4), 65–76.

Johnson, G. C., and M. J. McPhaden (1999), Interior pycnocline flow from the subtropical to the equatorial Pacific Ocean, *J. Phys. Oceanogr.*, *29*(12), 3073–3089.
Johnson, G. C., B. M. Sloyan, W. S. Kessler, and K. E. McTaggart (2002), Direct measurements of upper ocean currents and water properties across the tropical Pacific during the 1990s, *Prog. Oceanogr.*, *52*(1), 31–61, doi:10.1016/S0079-6611(02)00021-6.
Johnson, K., R. Gordon, and K. Coale (1997), What controls dissolved iron concentrations in the world ocean?, *Mar. Chem.*, *57*(3–4), 137–161.
Johnson, K., F. Chavez, and G. Friederich (1999), Continental-shelf sediment as a primary source of iron for coastal phytoplankton RID F-9742-2011, *Nature*, *398*(6729), 697–700.
Jones, M. T., C. R. Pearce, C. Jeandel, S. R. Gislason, E. S. Eiriksdottir, V. Mavromatis, and E. H. Oelkers (2012), Riverine particulate material dissolution as a significant flux of strontium to the oceans, *Earth Planet. Sci. Lett.*, *355–356*, 51–59, doi:10.1016/j.epsl.2012.08.040.
Kashino, Y., M. Aoyama, T. Kawano, N. Hendiarti, Syaefudin, Y. Anantasena, K. Muneyama, and H. Watanabe (1996), The water masses between Mindanao and New Guinea, *J. Geophys. Res.*, *101*(C5), 12,391–12,400, doi:10.1029/95JC03797.
Kineke, G., K. Woolfe, S. Kuehl, J. Milliman, T. Dellapenna, and R. Purdon (2000), Sediment export from the Sepik River, Papua New Guinea: Evidence for a divergent sediment plume, *Cont. Shelf Res.*, *20*(16), 2239–2266.
Kuehl, S. A. (2004), Nature of sediment dispersal off the Sepik River, Papua New Guinea: Preliminary sediment budget and implications for margin processes, *Cont. Shelf Res.*, *24*(19), 2417, doi:10.1016/j.csr.2004.07.016.
Lacan, F., and C. Jeandel (2001), Tracing Papua New Guinea imprint on the central Equatorial Pacific Ocean using neodymium isotopic compositions and Rare Earth Element patterns, *Earth Planet. Sci. Lett.*, *186*(3–4), 497–512.
Lacan, F., and C. Jeandel (2005), Neodymium isotopes as a new tool for quantifying exchange fluxes at the continent–ocean interface, *Earth Planet. Sci. Lett.*, *232*(3–4), 245–257, doi:10.1016/j.epsl.2005.01.004.
Lacan, F., A. Radic, C. Jeandel, F. Poitrasson, G. Sarthou, C. Pradoux, and R. Freydier (2008), Measurement of the isotopic composition of dissolved iron in the open ocean, *Geophys. Res. Lett.*, *35*, L24601, doi:10.1029/2008GL035736.
Lacan, F., A. Radic, M. Labatut, C. Jeandel, F. Poitrasson, G. Sarthou, C. Pradoux, J. Chmeleff, and R. Freydier (2010), High-precision determination of the isotopic composition of dissolved iron in iron depleted seawater by Double Spike Multicollector-ICPMS, *Anal. Chem.*, *82*(17), 7103–7111.
Landing, W. M., and S. Westerlund (1988), The solution chemistry of iron(II) in Framvaren Fjord, *Mar. Chem.*, *23*(3–4), 329–343.
Lindstrom, E., R. Lukas, R. Fine, E. Firing, S. Godfrey, G. Meyers, and M. Tsuchiya (1987), The Western Equatorial Pacific Ocean circulation study, *Nature*, *330*(6148), 533–537, doi:10.1038/330533a0.
Lindstrom, E., J. Butt, R. Lukas, and S. Godfrey (1990), The Flow through Vitiaz Strait and St. George's Channel, Papua New Guinea, in *The Physical Oceanography of Sea Straits*, edited by L. J. Pratt, pp. 171–189, Kluwer Academic Publishers, Netherlands.
Little, S. H., D. Vance, M. Siddall, and E. Gasson (2013), A modeling assessment of the role of reversible scavenging in controlling oceanic dissolved Cu and Zn distributions, *Global Biogeochem. Cycles*, *27*, 780–791, doi:10.1002/gbc.20073.
Lohan, M., A. Aguilar-Islas, R. Franks, and K. Bruland (2005), Determination of iron and copper in seawater at pH 1.7 with a new commercially available chelating resin, NTA Superflow, *Anal. Chim. Acta*, *530*(1), 121–129.
Lukas, R., and E. Firing (1984), The geostrophic balance of the Pacific Equatorial Undercurrent, *Deep Sea Res. Part A*, *31*(1), 61–66.
Luo, C., N. Mahowald, T. Bond, P. Y. Chuang, P. Artaxo, R. Siefert, Y. Chen, and J. Schauer (2008), Combustion iron distribution and deposition, *Global Biogeochem. Cycles*, *22*, GB1012, doi:10.1029/2007GB002964.
Mackey, D. J., J. E. O'Sullivan, and R. J. Watson (2002), Iron in the western Pacific: A riverine or hydrothermal source for iron in the Equatorial Undercurrent?, *Deep Sea Res., Part I*, *49*(5), 877–893.
Majestic, B. J., A. D. Anbar, and P. Herckes (2009a), Elemental and iron isotopic composition of aerosols collected in a parking structure, *Sci. Total Environ.*, *407*(18), 5104–5109.
Majestic, B. J., A. D. Anbar, and P. Herckes (2009b), Stable isotopes as a tool to apportion atmospheric iron, *Environ. Sci. Technol.*, *43*(12), 4327–4333.
Martin, J. H. (1990), Glacial-interglacial CO_2 change: The iron hypothesis, *Paleoceanography*, *5*(1), 1–13, doi:10.1029/PA005i001p00001.
Martin, J. H., R. M. Gordon, S. Fitzwater, and W. W. Broenkow (1989), Vertex: Phytoplankton/iron studies in the Gulf of Alaska, *Deep Sea Res. Part A*, *36*(5), 649–680.
Melet, A., L. Gourdeau, W. S. Kessler, J. Verron, and J.-M. Molines (2010), Thermocline circulation in the Solomon Sea: A modeling study, *J. Phys. Oceanogr.*, *40*(6), 1302–1319, doi:10.1175/2009JPO4264.1.
Menard, H. W., and S. M. Smith (1966), Hypsometry of ocean basin provinces, *J. Geophys. Res.*, *71*(18), 4305–4325, doi:10.1029/JZ071i018p04305.
Milliman, J. D., K. L. Farnsworth, and C. S. Albertin (1999), Flux and fate of fluvial sediments leaving large islands in the East Indies, *J. Sea Res.*, *41*(1–2), 97–107.
Moore, J., and O. Braucher (2008), Sedimentary and mineral dust sources of dissolved iron to the world ocean, *Biogeosciences*, *5*(3), 631–656.
Moore, J. K., S. C. Doney, and K. Lindsay (2004), Upper ocean ecosystem dynamics and iron cycling in a global three-dimensional model, *Global Biogeochem. Cycles*, *18*, GB4028, doi:10.1029/2004GB002220.
Murray, J. W., L. Balistrieri, B. Paul, B. Nelson, J. Laydbak, and G. J. Brunskill (2010), *56Fe in Surface Sediments From the Northeast Margin of Papua New Guinea as a Tracer for the Origin of Iron to the EUC*, Ocean Science Meeting, Portland.
Nozaki, Y., and D. S. Alibo (2003), Importance of vertical geochemical processes in controlling the oceanic profiles of dissolved rare earth elements in the northeastern Indian Ocean, *Earth Planet. Sci. Lett.*, *205*(3–4), 155–172, doi:10.1016/S0012-821X(02)01027-0.
Obata, H., K. Shitashima, K. Isshik, and E. Nakayama (2008), Iron, manganese and aluminum in upper waters of the western South Pacific ocean and its adjacent seas, *J. Oceanogr.*, *64*(2), 233–245.
Pickard, G. L., and W. J. Emery (1990), *Descriptive Physical Oceanography: An Introduction*, Elsevier, Boston, Mass.
Poitrasson, F. (2006), On the iron isotope homogeneity level of the continental crust, *Chem. Geol.*, *235*(1–2), 195–200.
Poitrasson, F., and R. Freydier (2005), Heavy iron isotope composition of granites determined by high resolution MC-ICP-MS, *Chem. Geol.*, *222*(1–2), 132–147.
Poitrasson, F., J. Viers, F. Martin, and J.-J. Braun (2008), Limited iron isotope variations in recent lateritic soils from Nsimi, Cameroon: Implications for the global Fe geochemical cycle, *Chem. Geol.*, *253*(1–2), 54–63, doi:10.1016/j.chemgeo.2008.04.011.
Poitrasson, F., et al. (2014), Iron isotope composition of the bulk waters and sediments from the Amazon River Basin, *Chem. Geol.*, *377*, 1–11, doi:10.1016/j.chemgeo.2014.03.019.
Qu, T., and E. J. Lindstrom (2002), A climatological interpretation of the circulation in the Western South Pacific*, *J. Phys. Oceanogr.*, *32*(9), 2492–2508.
Qu, T., S. Gao, I. Fukumori, R. A. Fine, and E. J. Lindstrom (2009), Origin and pathway of Equatorial 13°C Water in the Pacific identified by a simulated passive tracer and its adjoint, *J. Phys. Oceanogr.*, *39*(8), 1836–1853.

Radic, A., F. Lacan, and J. W. Murray (2011), Iron isotopes in the seawater of the equatorial Pacific Ocean: New constraints for the oceanic iron cycle, *Earth Planet. Sci. Lett.*, *306*(1–2), 1–10.
Rouxel, O., W. Shanks, W. Bach, and K. Edwards (2008a), Integrated Fe- and S-isotope study of seafloor hydrothermal vents at East Pacific rise 9–10 degrees N, *Chem. Geol.*, *252*(3–4), 214–227.
Rouxel, O., E. Sholkovitz, M. Charette, and K. Edwards (2008b), Iron isotope fractionation in subterranean estuaries, *Geochim. Cosmochim. Acta*, *72*(14), 3413–3430, doi:10.1016/j.gca.2008.05.001.
Rowe, G. D., E. Firing, and G. C. Johnson (2000), Pacific Equatorial subsurface countercurrent velocity, transport, and potential vorticity, *J. Phys. Oceanogr.*, *30*(6), 1172–1187.
Ryan, J. P., I. Ueki, Y. Chao, H. Zhang, P. S. Polito, and F. P. Chavez (2006), Western Pacific modulation of large phytoplankton blooms in the central and eastern equatorial Pacific, *J. Geophys. Res.*, *111*, G02013, doi:10.1029/2005JG000084.
Sedwick, P. N., E. R. Sholkovitz, and T. M. Church (2007), Impact of anthropogenic combustion emissions on the fractional solubility of aerosol iron: Evidence from the Sargasso Sea, *Geochem. Geophys. Geosyst.*, *8*, Q10Q06, doi:10.1029/2007GC001586.
Severmann, S., C. M. Johnson, B. L. Beard, C. R. German, H. N. Edmonds, H. Chiba, and D. R. H. Green (2004), The effect of plume processes on the Fe isotope composition of hydrothermally derived Fe in the deep ocean as inferred from the Rainbow vent site, Mid-Atlantic Ridge, 36°14′N, *Earth Planet. Sci. Lett.*, *225*(1–2), 63–76.
Severmann, S., C. Johnson, B. Beard, and J. McManus (2006), The effect of early diagenesis on the Fe isotope compositions of porewaters and authigenic minerals in continental margin sediments, *Geochim. Cosmochim. Acta*, *70*(8), 2006–2022.
Severmann, S., J. McManus, W. Berelson, and D. Hammond (2010), The continental shelf benthic iron flux and its isotope composition, *Geochim. Cosmochim. Acta*, *74*(14), 3984–4004.
Shank, L. M., and A. M. Johansen (2008), *Atmospheric Trace Metal and Labile Iron Deposition Fluxes to the Equatorial Pacific During EUCFe2006*, Ocean Sciences Meeting, Orlando.
Sharma, M., M. Polizzotto, and A. Anbar (2001), Iron isotopes in hot springs along the Juan de Fuca Ridge, *Earth Planet. Sci. Lett.*, *194*(1–2), 39–51.
Sholkovitz, E. R., H. Elderfield, R. Szymczak, and K. Casey (1999), Island weathering: River sources of rare earth elements to the Western Pacific Ocean, *Mar. Chem.*, *68*(1–2), 39–57.
Slemons, L., T. Gorgues, O. Aumont, C. Menkes, and J. W. Murray (2009), Biogeochemical impact of a model western iron source in the Pacific Equatorial Undercurrent, *Deep Sea Res., Part I*, *56*(12), 2115–2128.
Slemons, L., B. Paul, J. Resing, and J. W. Murray (2012), Particulate iron, aluminum, and manganese in the Pacific equatorial undercurrent and low latitude western boundary current sources, *Mar. Chem.*, *142–144*, 54–67.
Slemons, L. O., J. W. Murray, J. Resing, B. Paul, and P. Dutrieux (2010), Western Pacific coastal sources of iron, manganese, and aluminum to the Equatorial Undercurrent, *Global Biogeochem. Cycles*, *24*, GB3024, doi:10.1029/2009GB003693.
Smith, K. L., B. H. Robison, J. J. Helly, R. S. Kaufmann, H. A. Ruhl, T. J. Shaw, B. S. Twining, and M. Vernet (2007), Free-drifting icebergs: Hot spots of chemical and biological enrichment in the Weddell Sea, *Science*, *317*(5837), 478–482.
Sokolov, S., and S. R. Rintoul (2007), On the relationship between fronts of the Antarctic Circumpolar Current and surface chlorophyll concentrations in the Southern Ocean, *J. Geophys. Res.*, *112*, C07030, doi:10.1029/2006JC004072.
Staubwasser, M., F. von Blanckenburg, and R. Schoenberg (2006), Iron isotopes in the early marine diagenetic iron cycle, *Geology*, *34*(8), 629–632.
Staubwasser, M., R. Schoenberg, F. von Blanckenburg, S. Krueger, and C. Pohl (2013), Isotope fractionation between dissolved and suspended particulate Fe in the oxic and anoxic water column of the Baltic Sea, *Biogeosciences*, *10*(1), 233–245.
Stemmann, L., G. A. Jackson, and D. Ianson (2004), A vertical model of particle size distributions and fluxes in the midwater column that includes biological and physical processes - Part I: Model formulation, *Deep Sea Res., Part I*, *51*(7), 865–884, doi:10.1016/j.dsr.2004.03.001.
Strelow, F. W. E. (1980), Quantitative separation of gallium from zinc, copper, indium, iron(III) and other elements by cation-exchange chromatography in hydrobromic acid–acetone medium, *Talanta*, *27*(3), 231–236.
Tachikawa, K., V. Athias, and C. Jeandel (2003), Neodymium budget in the modern ocean and paleo-oceanographic implications, *J. Geophys. Res.*, *108*(C8), 3254, doi:10.1029/1999JC000285.
Tachikawa, K., O. Cartapanis, L. Vidal, L. Beaufort, T. Barlyaeva, and E. Bard (2011), The precession phase of hydrological variability in the Western Pacific Warm Pool during the past 400 ka, *Quat. Sci. Rev.*, *30*(25–26), 3716–3727.
Tagliabue, A., L. Bopp, O. Aumont, and K. Arrigo (2009), Influence of light and temperature on the marine iron cycle: From theoretical to global modeling, *Global Biogeochem. Cycles*, 23, *GB2017*, doi:10.1029/2008GB003214.
Tagliabue, A., et al. (2010), Hydrothermal contribution to the oceanic dissolved iron inventory, *Nat. Geosci.*, *3*(4), 252–256.
Talley, L. D. (1993), Distribution and Formation of North Pacific Intermediate Water, *J. Phys. Oceanogr.*, *23*(3), 517–537.
Teng, F.-Z., N. Dauphas, S. Huang, and B. Marty (2013), Iron isotopic systematics of oceanic basalts, *Geochim. Cosmochim. Acta*, *107*, 12–26, doi:10.1016/j.gca.2012.12.027.
Tomczak, M., and J. S. Godfrey (2003), *Regional Oceanography: An Introduction*, Elsevier Sci., Oxford.
Tomczak, M., and D. Hao (1989), Water masses in the thermocline of the Coral Sea, *Deep Sea Res. Part A*, *36*(10), 1503–1514.
Tsuchiya, M. (1981), The origin of the Pacific Equatorial 13 °C Water, *J. Phys. Oceanogr.*, *11*, 794–812.
Tsuchiya, M., and L. D. Talley (1998), A Pacific hydrographic section at 88°W: Water-property distribution, *J. Geophys. Res.*, *103*(C6), 12,899–12,918, doi:10.1029/97JC03415.
Tsuchiya, M., R. Lukas, and R. Fine (1989), Source waters of the Pacific equatorial undercurrent, *Prog. Oceanogr.*, *23*, 101–147.
Turner, D. R., and K. A. Hunter (2001), *The Biogeochemistry of Iron in Seawater*, John Wiley, Chichester, U. K.
Urey, H. C. (1947), The thermodynamic properties of isotopic substances, *J. Chem. Soc.*, *0*, 562–581, doi:10.1039/JR9470000562.
Ussher, S., E. Achterberg, and P. Worsfold (2004), Marine biogeochemistry of iron, *Environ. Chem.*, *1*(2), 67–80.
Waeles, M., A. Baker, T. Jickells, and J. Hoogewerff (2007), Global dust teleconnections: Aerosol iron solubility and stable isotope composition, *Environ. Chem.*, *4*(4), 233–237.
Walsh, J., and C. Nittrouer (2003), Contrasting styles of off-shelf sediment accumulation in New Guinea, *Mar. Geol.*, *196*(3–4), 105–125, doi:10.1016/S0025-3227(03)00069-0.
Windom, H. L., W. S. Moore, L. F. H. Niencheski, and R. A. Jahnke (2006), Submarine groundwater discharge: A large, previously unrecognized source of dissolved iron to the South Atlantic Ocean, *Mar. Chem.*, *102*(3–4), 252–266.
Woodhead, J., J. Hergt, M. Sandiford, and W. Johnson (2010), The big crunch: Physical and chemical expressions of arc/continent collision in the Western Bismarck arc, *J. Volcanol. Geotherm. Res.*, *190*(1–2), 11–24.
Wu, J., Z. Liu, and C. Zhou (2013), Provenance and supply of Fe-enriched terrigenous sediments in the western equatorial Pacific and their relation to precipitation variations during the late Quaternary, *Global Planet. Change*, *108*, 56–71.

Wu, J. F., and E. Boyle (2002), Iron in the Sargasso Sea: Implications for the processes controlling dissolved Fe distribution in the ocean, *Global Biogeochem. Cycles*, *16*(4), 1086, doi:10.1029/2001GB001453.

Wyrtki, K., and B. Kilonsky (1984), Mean water and current structure during the Hawaii-to-Tahiti shuttle experiment, *J. Phys. Oceanogr.*, *14*, 242–254.

You, Y. (2003), The pathway and circulation of North Pacific Intermediate Water, *Geophys. Res. Lett.*, *30*(24), 2291, doi:10.1029/2003GL018561.